Deskripsi Artikel

- Judul Jurnal : TEKNOSAINS: Jurnal Sains, Teknologi dan Informatika
- Volume Jurnal : Volume 11, Nomor 2, July 2024
- Akreditasi : Peringkat 4
- Judul Artikel : Effect of buoyancy force on buoyancy waterwheel efficiency using numerical flow simulation
- Penulis : Fadhlurrahman Zaki, **Dan Mugisidi**.
- Status Penulis : Kontributor

SERTIFIKAT

Direktorat Jenderal Pendidikan Tinggi, Riset dan Teknologi
Kementerian Pendidikan, Kebudayaan, Riset dan Teknologi Republik Indonesia

Kutipan dari Keputusan Direktorat Jenderal Pendidikan Tinggi, Riset dan Teknologi
Kementerian Pendidikan, Kebudayaan, Riset, dan Teknologi Republik Indonesia

Nomor 105/E/KPT/2022
Peringkat Akreditasi Jurnal Ilmiah Periode 1 Tahun 2022

Nama Jurnal Ilmiah

Teknosains : Jurnal Sains, Teknologi dan Informatika

E-ISSN: 27214729

Penerbit: Sekolah Tinggi Teknologi Muhammadiyah Cileungsi

Ditetapkan Sebagai Jurnal Ilmiah

TERAKREDITASI PERINGKAT 4

Akreditasi Berlaku selama 5 (lima) Tahun, yaitu
Volume 7 Nomor 1 Tahun 2020 Sampai Volume 11 Nomor 2 Tahun 2024

Jakarta, 07 April 2022
Plt. Direktur Jenderal Pendidikan Tinggi,
Riset, dan Teknologi

Prof. Ir. Nizam, M.Sc., DIC, Ph.D., IPU, ASEAN Eng
NIP. 196107061987101001

Balai Sertifikasi Elektronik

Catatan :
1. UU ITE No 11 Tahun 2008 Pasal 5 Ayat 1 "Informasi Elektronik dan/atau hasil cetakannya merupakan alat bukti yang sah"
2. Dokumen ini telah ditandatangani secara elektronik menggunakan sertifikat elektronik yang diterbitkan oleh BSrE

Editorial Team

https://jurnal.sttmcileungsi.ac.id/index.php/tekno/editorial

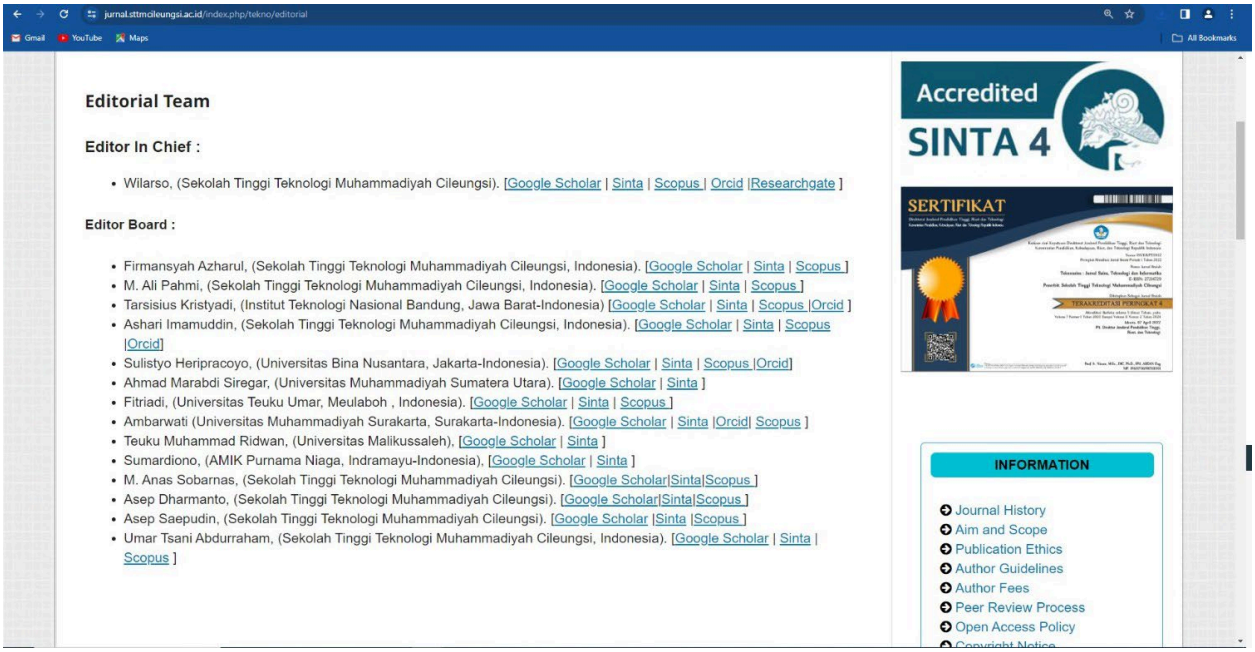

Editorial Team

Editor In Chief :

- Wilarso, (Sekolah Tinggi Teknologi Muhammadiyah Cileungsi). [Google Scholar | Sinta | Scopus | Orcid |Researchgate]

Editor Board :

- Firmansyah Azharul, (Sekolah Tinggi Teknologi Muhammadiyah Cileungsi, Indonesia). [Google Scholar | Sinta | Scopus]
- M. Ali Pahmi, (Sekolah Tinggi Teknologi Muhammadiyah Cileungsi, Indonesia). [Google Scholar | Sinta | Scopus]
- Tarsisius Kristyadi, (Institut Teknologi Nasional Bandung, Jawa Barat-Indonesia) [Google Scholar | Sinta | Scopus |Orcid]
- Ashari Imamuddin, (Sekolah Tinggi Teknologi Muhammadiyah Cileungsi, Indonesia). [Google Scholar | Sinta | Scopus |Orcid]
- Sulistyo Heripracoyo, (Universitas Bina Nusantara, Jakarta-Indonesia). [Google Scholar | Sinta | Scopus |Orcid]
- Ahmad Marabdi Siregar, (Universitas Muhammadiyah Sumatera Utara). [Google Scholar | Sinta]
- Fitriadi, (Universitas Teuku Umar, Meulaboh , Indonesia). [Google Scholar | Sinta | Scopus]
- Ambarwati (Universitas Muhammadiyah Surakarta, Surakarta-Indonesia). [Google Scholar | Sinta |Orcid| Scopus]
- Teuku Muhammad Ridwan, (Universitas Malikussaleh). [Google Scholar | Sinta]
- Sumardiono, (AMIK Purnama Niaga, Indramayu-Indonesia). [Google Scholar | Sinta]
- M. Anas Sobarnas, (Sekolah Tinggi Teknologi Muhammadiyah Cileungsi). [Google Scholar|Sinta|Scopus]
- Asep Dharmanto, (Sekolah Tinggi Teknologi Muhammadiyah Cileungsi). [Google Scholar|Sinta|Scopus]
- Asep Saepudin, (Sekolah Tinggi Teknologi Muhammadiyah Cileungsi). [Google Scholar |Sinta |Scopus]
- Umar Tsani Abdurraham, (Sekolah Tinggi Teknologi Muhammadiyah Cileungsi, Indonesia). [Google Scholar | Sinta | Scopus]

Accredited SINTA 4

SERTIFIKAT

INFORMATION

- Journal History
- Aim and Scope
- Publication Ethics
- Author Guidelines
- Author Fees
- Peer Review Process
- Open Access Policy

Daftar Isi

https://jurnal.sttmcileungsi.ac.id/index.php/tekno

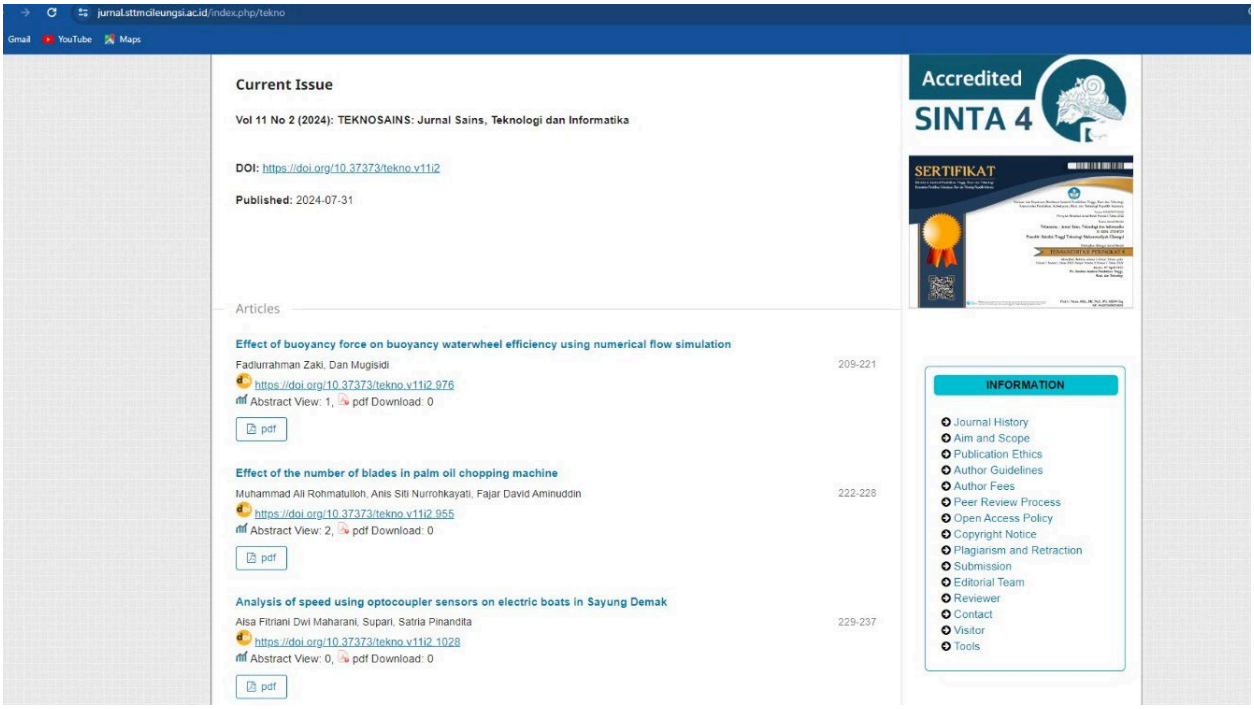

Current Issue

Vol 11 No 2 (2024): TEKNOSAINS: Jurnal Sains, Teknologi dan Informatika

DOI: https://doi.org/10.37373/tekno.v11i2

Published: 2024-07-31

Articles

Effect of buoyancy force on buoyancy waterwheel efficiency using numerical flow simulation 209-221

Fadlurrahman Zaki, Dan Mugisidi

https://doi.org/10.37373/tekno.v11i2.976

Abstract View: 1, pdf Download: 0

pdf

Effect of the number of blades in palm oil chopping machine 222-228

Muhammad Ali Rohmatulloh, Anis Siti Nurrohkayati, Fajar David Aminuddin

https://doi.org/10.37373/tekno.v11i2.955

Abstract View: 2, pdf Download: 0

pdf

Analysis of speed using optocoupler sensors on electric boats in Sayung Demak 229-237

Alsa Fitriani Dwi Maharani, Supari, Satria Pinandita

https://doi.org/10.37373/tekno.v11i2.1028

Abstract View: 0, pdf Download: 0

pdf

Accredited SINTA 4

SERTIFIKAT

INFORMATION

- Journal History
- Aim and Scope
- Publication Ethics
- Author Guidelines
- Author Fees
- Peer Review Process
- Open Access Policy
- Copyright Notice
- Plagiarism and Retraction
- Submission
- Editorial Team
- Reviewer
- Contact
- Visitor
- Tools

ISSN 2087-3336 (Print) | 2721-4729 (Online)
TEKNOSAINS: Jurnal Sains, Teknologi dan Informatika
Vol 11, No. 2, July 2024, page. 209-221
http://jurnal.sttmcileungsi.ac.id/index.php/tekno
DOI: 10.37373

Effect of buoyancy force on buoyancy waterwheel efficiency using numerical flow simulation

Fadhlurrahman Zaki, Dan Mugisidi*

* Mechanical Engineering, Faculty of Industrial Technology and Information Technology, Muhammadiyah University Prof. Dr. Hamka, Indonesia, 13830. Jl. Tanah Merdeka No.6, RT.10/RW.5 13830 Region of Jakarta, Indonesia

*✉ dan.mugisidi@uhamka.ac.id

Submitted: 30/12/2023 Revised: 15/01/2024 Accepted: 07/02/2024

ABSTRACT

In this work, the performance of a buoyant waterwheel to produce hydrokinetic power is investigated through analytical theory and computational fluid dynamics simulation. The impact of the buoyancy wheel is investigated by establishing the performance parameters through the use of a moving mesh approach and a realizable k-ε turbulence model. Transient simulation is required to comprehend the flow of physical processes. Using moving mesh as a transient methodology of the buoyancy waterwheel, numerical flow simulations and theoretical analytical methods are used in this study to assess the effect of buoyant force generated on the performance of the buoyancy wheel. The buoyancy waterwheel that will be put to the test has eight straight blades and a diameter of one meter. The pinwheel force and torque created in the numerical flow simulation (CFD) are 414.96 N and 207.48 Nm, respectively, whereas in the theoretical calculation, they are 449.06 N and 224.53 Nm, according to the research findings. It is possible to compute the buoyancy wheel's power output and efficiency mathematically, yielding values of 1619.35 W and 68.07%. The buoyancy wheel's power output and efficiency, as determined by numerical flow simulation, are 1495.95 W and 62.88%, respectively. Based on theoretical and CFD study results, the buoyancy wheel generates a standard deviation of 7.62%. Thus, for the buoyancy wheel, a temporary method that takes advantage of the moving mesh characteristic is advised. This method can also be applied as a future alternative energy source for the Piko hydro turbine.

Keywords: Renewable energy; waterwheel; CFD; moving mesh; hydropower

1. INTRODUCTION

Year after year, Indonesia's requirement for electrical energy keeps growing [1]. Because of the depletion of non-renewable natural resources, research is being done on the potential of renewable energy to provide electricity [2],[3]. Indonesia create renewable energy sources like hydro energy because it is a tropical nation [4],[5], wind energy [6]–[10], geothermal energy [11], biogas energy [12], and biomass energy [13]. Hydropower is regarded as a clean, sustainable energy source with enormous growth potential [14]. By 2025, the Indonesian government wants to use 23% renewable energy, particularly in the country's outlying regions [15]. Pico hydro is the term for water energy, which falls under the lowest size category and has a maximum production of 5 kW [16]. The process of operating a pico hydro water turbine involves using the turbine's rotation to generate mechanical energy [17]. An electric generator uses a revolving turbine to transform mechanical energy into electrical energy. Numerous varieties of hydraulic turbines exist: Reaction turbines (like Francis and Kaplan) employ water pressure, impulse turbines (like Pelton, Turgo, and Banki) use water kinetic energy, and gravity turbines (like water wheels and Archimedes screws) rely mostly on water weight [18],[19].

A great deal of research has been done to enhance turbine performance to solve this issue. William and Samson believe that a pico hydro turbine would be a wise decision [20], the feasibility analysis of self-sufficient electricity production for outlying areas. The effectiveness of waterwheels in connection to the ratio of immersion radius to paddle count was examined by Tevata and Inprasit. Their research indicates a significant relationship between the torque load of a waterwheel running at maximum power and the dipping radius ratio [21]. As stated by Quaranta [22]–[24], The efficacy of the breastshot waterwheel can be increased by numerically and experimentally altering the overshot waterwheel's geometry with a circular wall encircling the wheel. Warjito also examined the quantity of distinct buckets to evaluate the flow field's performance and quality. The efficiency of water wheels is expected to be significantly impacted by the design of the radial blades [25]. Next, Adanta assessed Warjito's proposal [25]. Each wheel's moment of inertia is determined using the CFD approach with 6-DoF characteristics. Thus, 20 blades get the best results, but 8 blades yield the most consistent results [26].

In the realm of renewable energy, the combination of buoyancy and water wheel is particularly promising for hydroelectric power plants [27]. In fluid mechanics, the upward force a fluid exerts on a submerged object is known as the buoyant force [28]. Archimedes' principle states that this force is equal to the weight of the fluid displaced by the submerged item [29]. This idea is particularly clear in fluids like water, where items float or have a reduced effective weight because buoyant force opposes gravity [30]. A submerged object's buoyant force is produced by the pressure differential between its top and bottom, with higher pressure at the bottom providing an upward push [31]. This means that new avenues for optimizing energy extraction from dynamic water settings are made possible by the strategic interaction of buoyancy forces with water wheels [32].

Compared to experimental and analytical techniques, CFD methods can depict the flow field in greater detail [33]. Moving Mesh was selected for the temporary method since it uses less processing resources and is frequently employed by researchers [34]–[36]. Using moving mesh as a transient methodology for buoyancy wheels, computational fluid dynamics (CFD) and theoretical analytical methods are used in this study to estimate the power and efficiency produced by buoyancy wheels.

2. METHOD

2.1. Governing equation

The following is equation (1) of continuity for incompressible fluids based on the rule of conservation of mass [37].

$$\frac{\partial \rho}{\partial t} + \frac{\partial \rho U_i}{\partial x_i} = 0 \tag{1}$$

The Navier-Stokes momentum equation, equation (2), can be computed as follows by applying the momentum conservation law:

$$\frac{\partial \rho U_i}{\partial t} + \frac{\partial \rho U_i U_j}{\partial x_j} = \frac{\partial \rho}{\partial x_i} + \frac{\partial}{\partial x_i}\left[(\mu + \mu_t)\left(\frac{\partial U_i}{\partial x_j} + \frac{\partial U_j}{\partial x_i}\right)\right] \tag{2}$$

where ρ represents the density of water, Ui the speed, t the time, and coordinates x_i and x_j, in addition to turbulence and molecular viscosity by μ and μ_t respectively.

2.1.1. VOF method

The distance between the free liquid level and the bed bottom in the multiphase flow module is represented by the VOF model, which investigates the gas-liquid interface in unpressurized flow as a two-phase flow problem. It is defined that the Navier-Stoke equations apply to uniformly incompressible fluids [38]:

$$\nabla \cdot \bar{u} = 0 \tag{3}$$

$$\frac{\partial \bar{u}}{\partial \mathrm{t}} + (\bar{u} \cdot \nabla)\bar{u} = -\frac{1}{\rho}\nabla \bar{p} + \mu \nabla^2 \bar{u} + \rho g \tag{4}$$

Where $\bar{u}$ denotes the speed, μ is the dynamic viscosity coefficient, $\bar{p}$ denotes pressure, ρ is the density of the fluid, and g represents the acceleration due to gravity. The location of the gas-liquid interface can be found by solving the volume fraction of each phase as follows:

$$\frac{\partial \alpha_q}{\partial t} + \frac{\partial \alpha_q \bar{u}_i}{\partial x_i} + \frac{\partial \alpha_q \bar{u}_j}{\partial x_j} + \frac{\partial \alpha_q \bar{u}_w}{\partial x_w} = 0 \quad (5)$$

Where α_q is the volume fraction of water from each grid? When α_q = 1, there is the same amount of water in the grid. There is no liquid in the grid if α_q = 0. when the air-water-free is in the range of 0 to 1. After determining the volume fraction of water α_q, hence the gas volume fraction α_p = 1 - α_q. Equation (6) determines the volume fraction, which is used to model the density and dynamic viscosity coefficients [39]:

$$\mu = \alpha_q \mu_q + (1 - \alpha_q)\mu_p \quad (6)$$

$$\rho = \alpha_q \rho_q + (1 - \alpha_q)\rho_p \quad (7)$$

2.1.2. k- ε turbulence model

An enhanced method is employed to compute the turbulent viscosity in the acceptable k-ε model. Using the proper transport equation of the fluctuating components' vortex strength, one can construct the dissipation rate equation. It is considered the k model is admissibly more accurate than the k-ε model in forecast the dissipation rate distribution of flat and spherical jets. Furthermore, plausible k-ε models allow for better predictions of boundary layer parameters at large pressure gradients and in separated and revolving flows [40]. The model's transport equations are each written as [40].

$$\frac{\partial}{\partial t}(\rho k) + \frac{\partial}{\partial t}(\rho k\, u_i) = \frac{\partial}{\partial x_i}\left[\left(\mu + \frac{u_t}{\sigma_k}\right)\frac{\sigma_k}{\sigma_{xj}}\right] + G_k + G_b - \rho\varepsilon - Y_M + S_k \quad (8)$$

$$\frac{\partial}{\partial t}(\rho \varepsilon) + \frac{\partial}{\partial t}(\rho \varepsilon\, u_i) = \frac{\partial}{\partial x_j}\left[\left(\mu + \frac{u_t}{\sigma_k}\right)\frac{\sigma_\varepsilon}{\sigma_{xj}}\right] + C_{1\varepsilon}\frac{\varepsilon}{k}(G_k + G_{3\varepsilon} + G_b) - C_{2\varepsilon}\rho\frac{\varepsilon^2}{k} + S_\varepsilon \quad (9)$$

2.2. Model matematika

A full-size flow buoyancy wheel consists of an eight-bladed, straight, basic wheel. Diagonal propellers are being created to perform better in future studies. The rational area and flow area of the waterwheel are mostly included in a 3D model that is built using CAD software. The water wheel measures 0.16 meters in width (b), 1 meter in outer diameter (D), 0.3 meters in hub diameter (d), 0.0018 meters in thickness (t) for the wheel blades, and 0.02 meters inside clearance. This optimizes the energy in motion. Waterwheels are made of aluminum type 6061, which has a density of 2700 kg/m^3. The general design specifications are shown in Table 1. Figure 1 shows the test model design for the buoyancy wheel operation.

Table 1. Buoyancy wheel design parameters

Design parameters	Value
Rated output power, P_{rated} (kW)	1.3
The outer radius of the wheel, R (m)	0.5
Waterwheel width, b (m)	0.16
Blade dimensions (m) (Length x Width x Thickness)	0.00345 x 0.15 x 0.0018
Blade shape	Rectangle

For the analytical design of the water wheel, the researchers provided technical background. Cornelis defines the power output of a water wheel as Equation (10) [41]:

$$P_{out} = \tau \cdot \omega \quad (10)$$

Where T shows the torque and angular speed of the water wheel. Plotkin describes the resulting torque in Equation (11) [42]:

$$\tau = F \cdot \frac{D}{2} \tag{11}$$

Equation (10) added to Equation (11) will produce equation (12) [43]:

$$P_{out} = F \cdot \omega \cdot \frac{D}{2} \tag{12}$$

Floating water wheels are designed to operate in both air and water zones, as seen in Figure 2. Figure 2 shows a floating water wheel with a free-body diagram representing the ambient conditions and working forces. The buoyant force of the air in the water zone and the gravity of the water in the air zone are what cause this water wheel to circle. The water wheel is turned by the torque created by the water-filled bucket falling through the air [24]. There is more air trapped in bucket 4 than water when it reaches bucket 5 in position. Because of this, the combined bucket's density is less than that of water, creating a buoyant force (Fb). This process is repeated for all eight buckets, leaving four in the various work zones with water and four with air inside [44]. The combined weight of the water and the air's lifting force generates the torque and power that the water wheel produces as it rotates [45]. The following equations (14)–(21) can be used to compute the force applied to the floating water wheel.

$$d_{shaft} = \sqrt[3]{\frac{16 \cdot \tau_{max} \cdot FS}{\pi \cdot \sigma_{yield}}} \tag{13}$$

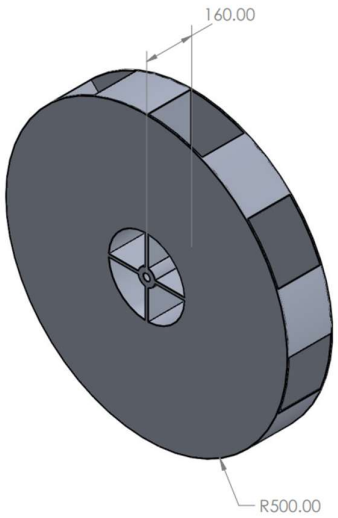

Figure 1. 3D model design of the buoyancy wheel

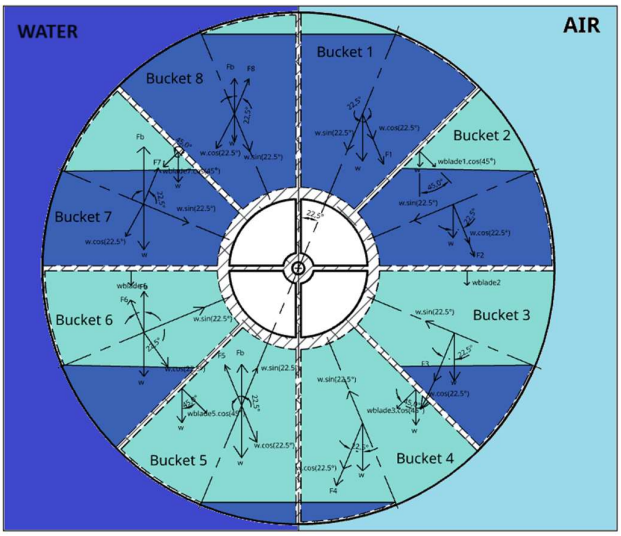

Figure 2. Free body diagram of the buoyancy wheel

The buoyancy wheel is designed to work in both air and water zones, as seen in Figure 2. Figure 2 shows a buoyancy wheel with a free-body diagram representing the working forces and ambient conditions. The buoyant force of the air in the water zone and the gravity of the water in the air zone are what cause this water wheel to circle. The water wheel is turned by the torque created by the water-filled bucket falling through the air [24]. There is more air trapped in bucket 4 than water when it reaches bucket 5 in position. Because of this, the combined bucket's density is less than that of water, creating a buoyant force (Fb). This process is repeated for all eight buckets, leaving four in the various work zones with water and four with air inside [44]. The combined weight of the water and the air's lifting force generates the torque and power that the water wheel produces as it rotates [45]. The force exerted on the buoyancy wheel can be calculated using equations (14)-(21) below.

$$F_1 = w \cdot \cos\theta = (m_{air} \cdot \cos 22.5° + m_{blade} \cdot \cos 45°) \cdot g \tag{14}$$

$$F_2 = w \cdot \cos\theta = (m_{air} \cdot \cos 22.5° + m_{blade}) \cdot g \quad (15)$$

$$F_3 = w \cdot \cos\theta = (m_{air} \cdot \cos 22.5° + m_{blade} \cdot \cos 45°) \cdot g \quad (16)$$

$$F_4 = w \cdot \cos\theta = (m_{water} \cdot \cos 45°) \cdot g \quad (17)$$

$$F_5 = \rho_{water} \cdot g \cdot V_{bucket} \cdot \cos 22.5° - \rho_{material} \cdot g \cdot V_{blade} \cdot \cos 45° \quad (18)$$

$$F_6 = \rho_{water} \cdot g \cdot V_{bucket} \cdot \cos 22.5° - \rho_{material} \cdot g \cdot V_{blade} \quad (19)$$

$$F_7 = \rho_{water} \cdot g \cdot V_{bucket} \cdot \cos 22.5° - \rho_{material} \cdot g \cdot V_{blade} \cdot \cos 45° \quad (20)$$

$$F_8 = \rho_{water} \cdot g \cdot V_{bucket} \cdot \cos 22.5° \quad (21)$$

To making the moment of inertia calculation easier, it is assumed that the water wheel is straight. At that point, the waterwheel bucket can be roughly modeled as a solid cylinder [46]. where m is the water wheel's mass and r is its outer radius. Therefore, using equation (22) the buoyancy wheel's inertia can be computed as follows [47]:

$$I = \frac{1}{2} \cdot m \cdot r^2 = \frac{1}{2} \rho \cdot V \cdot r^2 \quad (22)$$

Equations (23) and (24) are used to determine the angular velocity (ω) and wheel speed respectively [48],[49]:

$$\omega = \frac{2\pi \cdot N}{60} \quad (23)$$

$$v = \omega \cdot r \quad (24)$$

where N is the turbine revolutions per minute. Equation (25) is used to calculate the input power (P_{in}) [50]:

$$P_{in} = \rho \cdot g \cdot Q \cdot H \quad (25)$$

Where Q is discharge, H is head, ρ is water density and g is acceleration caused by gravity. Equation (26) is the ratio of the power available at the shaft (P_{out}) to input power (P_{in}) called hydraulic efficiency (η) [51]:

$$\eta = \frac{P_{out}}{P_{in}} \quad (26)$$

2.3. Boundary conditions and simulation setup

As seen in Figure 3, boundary conditions (BC) define a rotating domain and a static domain. In the rotational domain, the water wheel is set up as a wall-type BC, and the k-ε turbulence model used in this simulation is derived from earlier studies on picohydro water turbines conducted by different researchers [52]. Since this simulation is multiphase, the rotating domain is where fluids like air and water are defined [53]. Both have a zero-speed initialization. Water and air were once half-domains that were both stationary and rotating. Domain gravity is 9.81 m/s about the suitable coordinate system [54]. The right-hand rule states that throughout domain movement, the domain will spin at a constant speed of 69 revolutions per minute. Numerous boundary conditions (BCs) are provided, such as zero outlet pressure, one meter per second (m/s) input velocity for air 0.121 m^3/s for water utilizing Qin, and non-slip wall boundary conditions. In a similar vein, it is believed that the domain's surface facing the atmosphere serves as a symmetric border condition. Inner and outer interfaces link the spinning and stationary domains [49].

P-V coupling is handled by the SIMPLE scheme, momentum is handled by the Body Force Weighted for Pressure scheme, and spatial discretization is handled by the 2nd-order upwind scheme [55]. The convergence criteria of the turbulence equations, momentum, and continuity requirements are satisfied by the values 1×10^{-4} [56]. An implicit scheme is used to calculate the volume fraction. To achieve a balance between accuracy and efficiency, the simulation time for each time step is set to 20 iterations. A time step size of 0.025s was chosen for transient simulation.

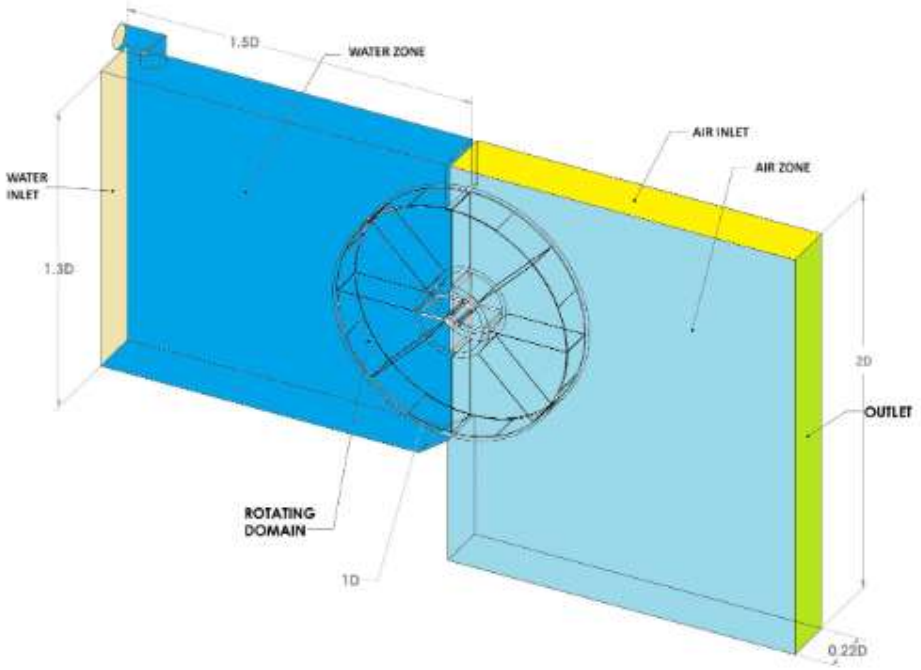

Figure 3. Boundary conditions for the buoyancy wheel simulation setup.

2.4. Grid independency test

A three-dimensional (3D) model of the water wheel and the surrounding flow field domain is created to compare with the analytical results. The characteristics and performance of the buoyancy wheel were analyzed using ANSYS 18.1. The wheel and fluid domains use tetrahedral meshes due to the complexity of the system [57]. The goal of the Grid Independence Test is to ensure that the results do not depend on additional grid refinements [58]. The grid Independence Test is a technique to reduce computing time and costs by avoiding using the best grid. The test-independent grid can be said to have converged if the error is less than 1% [59], [60]. Numerical analysis was performed and five grids with varying degrees of fineness were created in this study. By plotting torque results against the number of elements in a particular mesh type, the Grid Independence Test shows that grid size significantly influences turbine torque performance. From Figure 4 it can be seen that a mesh with 0.57 million elements produces almost the same power results as a mesh with 0.86 million elements and the mesh distribution used is shown in Figure 5. Therefore, to get accurate results with less time and computational costs in this study, a mesh with 0.57 million elements was used for this simulation.

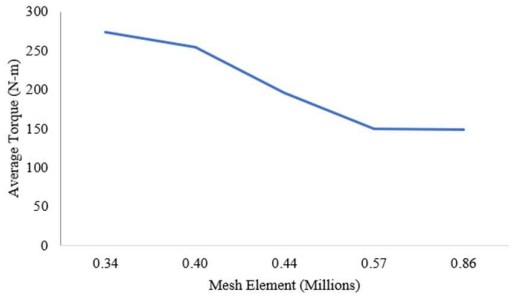

Figure 4. Effect of grid refinement on the torque produced by the turbine

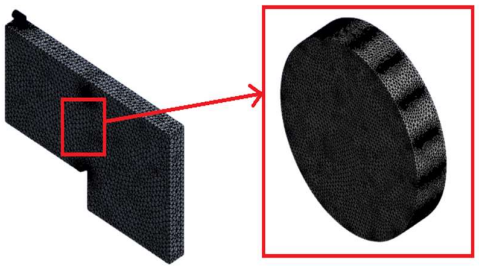

Figure 5. Visualization of 0.57 million mesh elements

3. RESULTS AND DISCUSSION

3.1. Theoretical analysis results

First estimates of the water resources at the mechanical engineering laboratory were used to build the buoyancy wheel, which has a 2 m head and a 0.121 m^3/s water output. Equations (14)–(17) are used to determine the buoyancy force components while equations (18)–(21) are used to calculate the gravity components of the buoyancy wheel (Figure 2). Table 2 and Figure 6 exhibit the style analysis's findings.

Table 2. Analysis of the forces acting on the buoyancy wheel

No. Bucket	Force (N)
Bucket 1	115.98
Bucket 2	91.33
Bucket 3	32.39
Bucket 4	5.02
Bucket 5	4.26
Bucket 6	26.46
Bucket 7	86.26
Bucket 8	87.37
Total	449.06

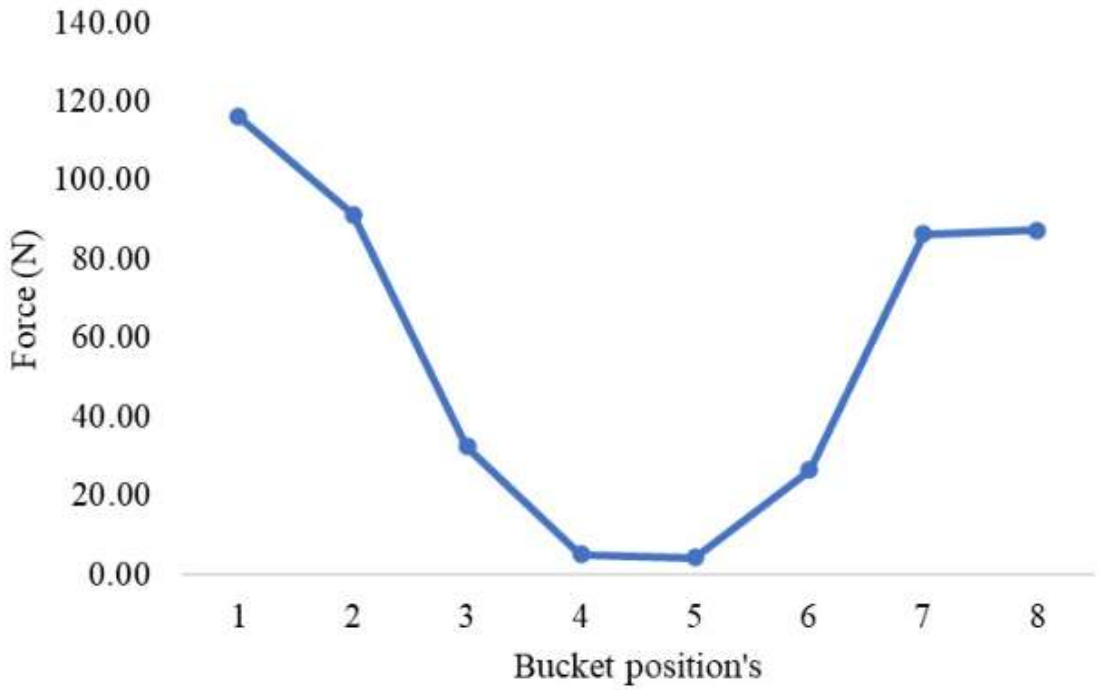

Figure 6. Forces acting on a floating waterwheel.

Equation (11) is used to compute the buoyancy wheel's torque component, which equals 224.53 N-m when the force produced by the buoyancy wheel's radius is multiplied. Equations (22), (23), (13), and (24) are used to compute the moment of inertia (I), angular velocity (ω), shaft diameter (do), and buoyancy wheel speed (v) from the buoyancy wheel design. Table 3 displays the findings of the parameter data.

Table 3. Several parameters that work on the buoyancy wheel

Parameters	Value
Moment of Inertia, I ($kg.m^2$)	4.31
Rotation speed, ω, (rad/s)	7.21
Shaft diameter, d_o (mm)	30
Buoyancy wheel speed, v (m/s)	3.61

3.2. CFD analysis results

3.2.1. Effect of buoyancy force on buoyancy wheel performance

The water volume fraction in the eight buckets can function because of the difference in water height between the water and air zones, according to the simulation findings shown in Figure 7. The buoyancy wheel is operated by the force mechanisms of buoyancy and gravity. The findings demonstrated that as the amount of water held in the bucket rose, its buoyancy increased as well. The buoyancy wheel's air and water fluids have different specific gravities of 0.00123 and 0.998, respectively, which causes an increase in buoyancy force. When the air-filled bucket starts to enter the water zone, there is a difference in specific gravity that causes a buoyant force that pushes the bucket upward and causes the wheel to rotate. Every object submerged in a fluid, whether fully or partially, will experience an upward buoyant force equal to the weight of the fluid displaced by the object, according to Archimedes' Law [61].

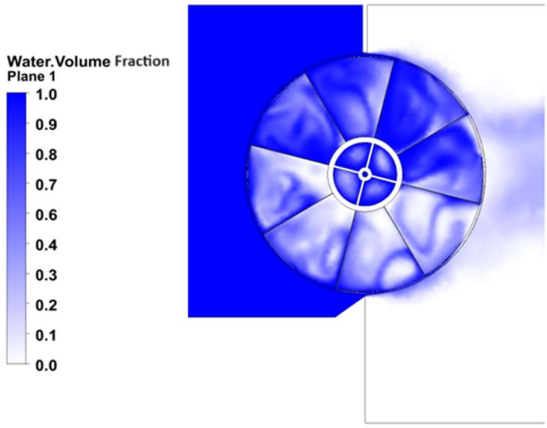

Figure 7. The volume fraction of water working on the buoyancy wheel.

3.2.2. Speed contours on the buoyancy wheel

Figure 8 further demonstrates that, throughout the majority of the domain width, the fluid velocity in the upstream region is constant. The downstream velocity profile, which also demonstrates that the fluid velocity is zero at the wall but changes rapidly across the width of the fluid domain due to the rotational motion of the turbine, indicates that the fluid velocity behind the turbine is lower due to the development of the wake region and the extraction of turbine kinetic energy from water molecules. After the water's kinetic energy is extracted by the turbine's buoyancy, the water's kinetic energy is diminished downstream, and the mechanical energy is accessible at the turbine shaft.

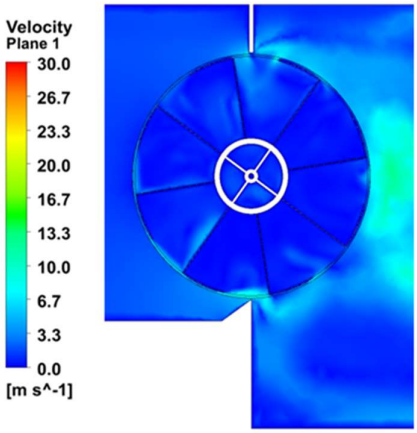

Figure 8. Buoyancy wheel speed contour

Simultaneously, a high-velocity zone appears at the advancing blade tip, indicating the dynamic nature of fluid dynamics during the simulation. Contour plots effectively highlight these variations, with red representing high speeds and blue depicting low speeds. This visual representation allows a clear

understanding of fluid behavior during turbine bucket rotation. Figure 8 shows the findings of the distribution of water flow velocity from each waterwheel bucket. With a maximum value of 30 m/s, the red color shows the area with the highest flow speed, while the light blue color shows the area with the lowest water flow speed, namely 3.3 m/s. The resulting buoyancy wheel speed is 3.6 m/s during this simulation.

3.3. Buoyancy wheel performance validation

It is possible to comprehend buoyancy wheel performance efficiency by employing numerical flow simulation analysis in conjunction with theoretical study. While computational analysis can offer a more comprehensive understanding of the factors influencing buoyancy wheel efficiency, numerical flow simulation analysis can offer a more accurate representation of the water flow surrounding a buoyancy wheel [62]. As demonstrated in Table 4, these two analytic methods can be used concurrently for more accurate findings. Equation (25) yields an input power (Pin) of 2378.99 W. In addition, 414.96 N of force and 207.48 N-m of torque are produced in the numerical flow simulation. The buoyancy wheel's performance efficiency can be computed using equation (26). It was discovered that the power generated by the numerical flow simulation analysis was 1495.95 W, while the power generated by the theoretical analysis utilizing equation (10) was 1619.35 W. In the numerical flow simulation, the buoyancy wheel produced an efficiency of 62.88%, but in the theoretical study, it was 68.07%. These findings show that the buoyancy wheel's performance created a 7.62% variance.

Table 4. Performance parameters on the buoyancy wheel

Parameter	Theoretical Results	CFD	Diff.
Power output, P_{out} (W)	1619.35	1495.95	0.0762
Eff. (%)	68.07%	62.88%	7.62%

4. SIMPULAN

Indonesia's annual demand for electrical energy is still rising. Research is being done on renewable energy as a source of energy for producing power because non-renewable natural resources are becoming scarce. It is appropriate to use CFD techniques to look into physical flow phenomena in the research of buoyancy wheels to completely comprehend the energy conversion process. Moving meshes are a common way for CFD algorithms to provide the boundary conditions for transient approximations for rotating case objects. Thus, using theoretical analysis techniques and CFD with moving mesh as a transient methodology for the buoyancy wheel, the goal of this research is to ascertain the impact of the ensuing buoyant force on the buoyancy wheel's performance. The force and torque generated by numerical calculations and simulations are 449.06 N and 224.53 Nm, respectively; 414.96 N and 207.48 Nm, according to the research findings. Additionally, the power generated by the numerical simulation and theoretical analysis is 1495.95 W and 1619.35 W, respectively. The buoyancy wheel generates an efficiency of 68.07% and 62.88%, yielding a 7.62% variance.

ACKNOWLEDGEMENT

Thank you to LEMLITBANG UHAMKA for funding this internal research with contract number 53/F.03.07/2022 and the Faculty of Industrial Technology and Information Technology (FTII) UHAMKA for facilitating research facilities and infrastructure.

REFERENCE

[1] D. Adanta, R. Fattah, and N. M. Muhammad, "COMPARISON OF STANDARD k-ε AND SST k-ωTURBULENCE MODEL FOR.pdf," *Mech. Sci. Eng.*, vol. 7, no. 2, pp. 39–44, 2020.

[2] P. Sritram and R. Suntivarakorn, "Comparative Study of Small Hydropower Turbine Efficiency at Low Head Water," *Energy Procedia*, vol. 138, pp. 646–650, 2017, doi: 10.1016/j.egypro.2017.10.181.

[3] O. D. Monsalve-Cifuentes, J. Graciano-Uribe, and D. A. H. Zuluaga, "Numerical Simulation of

a Propeller-Type Turbine for In-Pipe Installation," *J. Adv. Res. Fluid Mech. Therm. Sci.*, vol. 83, no. 1, pp. 1–16, 2021, doi: 10.37934/arfmts.83.1.116.

[4] A. W. Biantoro, I. Iskendar, S. Subekti, and N. H. Bin Muhd Noor, "The Effects of Water Debit and Number of Blades on the Power Generated of Prototype Turbines Propeller as Renewable Electricity," *J. Rekayasa Mesin*, vol. 12, no. 1, p. 203, 2021, doi: 10.21776/ub.jrm.2021.012.01.22.

[5] R. Klar, B. Steidl, and M. Aufleger, "A floating energy storage system based on fabric," *Ocean Eng.*, vol. 165, no. July, pp. 328–335, 2018, doi: 10.1016/j.oceaneng.2018.07.051.

[6] H. Im and B. Kim, "Power Performance Analysis Based on Savonius Wind Turbine Blade Design and Layout Optimization through Rotor Wake Flow Analysis," *Energies*, vol. 15, no. 24, 2022, doi: 10.3390/en15249500.

[7] M. Yusvika, A. Sutaji, A. R. Prabowo, F. Imaduddin, and S. Hadi, "Prediction of the Hydrodynamic Performance of an Elliptical Blade Savonius Turbine using Computational Fluid Dynamics," *IOP Conf. Ser. Mater. Sci. Eng.*, vol. 1096, no. 1, p. 012050, 2021, doi: 10.1088/1757-899x/1096/1/012050.

[8] F. D. Scheaua, "An alternative for wind energy conversion using improved Savonius rotor turbine model," *IOP Conf. Ser. Mater. Sci. Eng.*, vol. 1182, no. 1, p. 012069, 2021, doi: 10.1088/1757-899X/1182/1/012069.

[9] F. Balduzzi, A. Bianchini, R. Maleci, G. Ferrara, and L. Ferrari, "Critical issues in the CFD simulation of Darrieus wind turbines," *Renew. Energy*, vol. 85, pp. 419–435, 2016, doi: 10.1016/j.renene.2015.06.048.

[10] S. Susastro, A. Noerpamoengkas, M. Ulum, and G. Setyono, "Performance Analysis of Wind Power Generation Models Using Oscillating Water Column," *JRST (Jurnal Ris. Sains dan Teknol.*, vol. 4, no. 2, p. 57, 2020, doi: 10.30595/jrst.v4i2.6020.

[11] A. A. Ahmed, M. Assadi, A. Kalantar, T. Sliwa, and A. Sapińska-śliwa, "A Critical Review on the Use of Shallow Geothermal Energy Systems for Heating and Cooling Purposes," *Energies*, vol. 15, no. 12, pp. 1–23, 2022, doi: 10.3390/en15124281.

[12] M. J. B. Kabeyi and O. A. Olanrewaju, "Biogas Production and Applications in the Sustainable Energy Transition," *J. Energy*, vol. 2022, pp. 1–43, 2022, doi: 10.1155/2022/8750221.

[13] M. M. Tun, D. Juchelkova, M. M. Win, A. M. Thu, and T. Puchor, "Biomass energy: An overview of biomass sources, energy potential, and management in Southeast Asian countries," *Resources*, vol. 8, no. 2, 2019, doi: 10.3390/resources8020081.

[14] M. S. Güney and K. Kaygusuz, "Hydrokinetic energy conversion systems: A technology status review," *Renew. Sustain. Energy Rev.*, vol. 14, no. 9, pp. 2996–3004, 2010, doi: 10.1016/j.rser.2010.06.016.

[15] D. Mugisidi, I. N. Fauzi, O. Heriyani, Y. Djeli, E. Aidhilhan, and P. H. Gunawan, "Development of the Dethridge Wheel Blade Shape for Hydropower Generation in Irrigation Canals in Indonesia," *J. Adv. Res. Fluid Mech. Therm. Sci.*, vol. 98, no. 2, pp. 146–156, 2022, doi: 10.37934/arfmts.98.2.146156.

[16] F. B. Darsono, R. D. Widodo, Rusiyanto, and A. Nurdin, "Analysis Of the Effect of Flow Rate and Speed on Four Blade Tubular Water Bulb-Turbine Efficiency Using Numerical Flow Simulation," *J. Adv. Res. Fluid Mech. Therm. Sci.*, vol. 90, no. 2, pp. 1–8, 2022, doi: 10.37934/arfmts.90.2.18.

[17] E. Quaranta, J. P. Perrier, and R. Revelli, "Optimal design process of crossflow Banki turbines: Literature review and novel expeditious equations," *Ocean Eng.*, vol. 257, no. January, p. 111582, 2022, doi: 10.1016/j.oceaneng.2022.111582.

[18] E. Quaranta and R. Revelli, "Gravity water wheels as a micro hydropower energy source: A review based on historic data, design methods, efficiencies and modern optimizations," *Renew. Sustain. Energy Rev.*, vol. 97, no. November 2017, pp. 414–427, 2018, doi: 10.1016/j.rser.2018.08.033.

[19] D. K. Okot, "Review of small hydropower technology," *Renew. Sustain. Energy Rev.*, vol. 26, pp. 515–520, 2013, doi: 10.1016/j.rser.2013.05.006.

[20] A. A. Williams and R. Simpson, "Pico hydro - Reducing technical risks for rural electrification," *Renew. Energy*, vol. 34, no. 8, pp. 1986–1991, 2009, doi: 10.1016/j.renene.2008.12.011.

[21] A. Tevata and C. Inprasit, "The effect of paddle number and immersed radius ratio on water wheel performance," *Energy Procedia*, vol. 9, pp. 359–365, 2011, doi: 10.1016/j.egypro.2011.09.039.

[22] E. Quaranta and R. Revelli, "Hydraulic Behavior and Performance of Breastshot Water Wheels for Different Numbers of Blades," *J. Hydraul. Eng.*, vol. 143, no. 1, pp. 1–10, 2017, doi: 10.1061/(asce)hy.1943-7900.0001229.

[23] E. Quaranta and R. Revelli, "CFD simulations to optimize the blade design of water wheels," *Drink. Water Eng. Sci.*, vol. 10, no. 1, pp. 27–32, 2017, doi: 10.5194/dwes-10-27-2017.

[24] E. Quaranta and R. Revelli, "Output power and power losses estimation for an overshot water wheel," *Renew. Energy*, vol. 83, pp. 979–987, 2015, doi: 10.1016/j.renene.2015.05.018.

[25] Wariito, D. Adanta, S. A. Arifianto, S. B. Nasution, and Budiarso, "Effect of Blades Number on Undershot Waterwheel Performance with Variable Inlet Velocity," *Proc. - 2018 4th Int. Conf. Sci. Technol. ICST 2018*, no. 4749, pp. 1–6, 2018, doi: 10.1109/ICSTC.2018.8528714.

[26] Warjito, D. Adanta, Budiarso, and A. P. Prakoso, "The effect of bucketnumber on breastshot waterwheel performance," *IOP Conf. Ser. Earth Environ. Sci.*, vol. 105, no. 1, 2018, doi: 10.1088/1755-1315/105/1/012031.

[27] C. M. Wang, T. Utsunomiya, S. C. Wee, and Y. S. Choo, "Research on floating wind turbines: A literature survey," *IES J. Part A Civ. Struct. Eng.*, vol. 3, no. 4, pp. 267–277, 2010, doi: 10.1080/19373260.2010.517395.

[28] Mr. Shivakumar M, "The Law of Buoyancy Force," *Int. J. Eng. Res.*, vol. V5, no. 02, pp. 183–185, 2016, doi: 10.17577/ijertv5is020264.

[29] A. H. Alami, *General Concepts BT - Mechanical Energy Storage for Renewable and Sustainable Energy Resources*. 2020. [Online]. Available: http://www.springer.com/series/15883

[30] A. Nergaard, N. Architect, and P. Engineer, "The Magic of Buoyancy and Hydrostatics – Buoyancy and Effective Forces," *Mod. Appl. Sci.*, vol. 11, no. 12, p. 77, 2017, doi: 10.5539/mas.v11n12p77.

[31] T. Ozturk and A. Demirbas, "Electricity generation using water lifting force," *Energy Explor. Exploit.*, vol. 24, no. 4–5, pp. 285–296, 2006, doi: 10.1260/014459806779398794.

[32] A. H. Alami, "Analytical and experimental evaluation of energy storage using work of buoyancy force," *J. Renew. Sustain. Energy*, vol. 6, no. 1, 2014, doi: 10.1063/1.4866036.

[33] T. Kolšek, J. Duhovnik, and A. Bergant, "Simulation of unsteady flow and runner rotation during shut-down of an axial water turbine," *J. Hydraul. Res.*, vol. 44, no. 1, pp. 129–137, 2006, doi: 10.1080/00221686.2006.9521668.

[34] C. D. Widiawaty *et al.*, "Optimization of inverse-Prandtl of Dissipation in standard k-ε Turbulence Model for Predicting Flow Field of Crossflow Turbine," *CFD Lett.*, vol. 14, no. 1, pp. 112–127, 2022, doi: 10.37934/cfdl.14.1.112127.

[35] R. Pienika, G. Usera, and H. M. Ramos, "Simulation of a hydrostatic pressure machine with caffa3d solver: Numerical model characterization and evaluation," *Water (Switzerland)*, vol. 12, no. 9, 2020, doi: 10.3390/w12092419.

[36] A. G. P. Narrain, *Low head hydropower for local energy solutions*. 2017. doi: 10.1201/9781351182720.

[37] W. Feng, Y. Zheng, A. Yu, and Q. Tang, "Experimental and Numerical Analysis of the Clearance Effects between Blades and Hub in a Water Wheel Used for Power Generation," *Water*, vol. 14, no. 22, p. 3640, 2022, doi: 10.3390/w14223640.

[38] T. Bikmukhametov, "CFD Simulations of Multiphase Flows with Particles," Norwegian

University of Science and Technology, 2016. [Online]. Available: https://brage.bibsys.no/xmlui/handle/11250/2405984

[39] O. Elshawarby, "Computational Fluid Dynamics of Multiphase Flow Using ANSYS Fluent," 2021.

[40] H. Kheirkhah Gildeh, A. Mohammadian, I. Nistor, H. Qiblawey, and X. Yan, "CFD modeling and analysis of the behavior of 30° and 45° inclined dense jets - New numerical insights," *J. Appl. Water Eng. Res.*, vol. 4, no. 2, pp. 112–127, 2016, doi: 10.1080/23249676.2015.1090351.

[41] S. Cornelis, "Parametric study of the performance of an impulse-type turbine with CFD," 2015.

[42] K. V. Poletkin, "Calculation of magnetic force and torque between two arbitrarily oriented circular filaments using Kalantarov–Zeitlin's method," *Int. J. Mech. Sci.*, vol. 220, pp. 1–39, 2022, doi: 10.1016/j.ijmecsci.2022.107159.

[43] Z. Nurfadilah, D. Mugisidi, A. R. S. Pohan, and O. Heriyani, "Pengaruh Kincir Tertutup Terhadap Efisiensi dan Rugi-rugi," *Rekayasa Energi Manufaktur) J.* |, vol. 8, no. 1, pp. 2528–3723, 2023, [Online]. Available: http://doi.org/10.21070/rem.v8i1.1670

[44] E. Prihastuty and H. D. Harsono, "Perancangan Kincir Air Undershot Sebagai Penggerak Awal Pompa," *Mestro*, pp. 1–7, 2019, [Online]. Available: http://jurnal.untagcirebon.ac.id/index.php/mestro/article/view/27

[45] A. Syuriadi and A. Nidhar, "Pengujian variasi jumlah dan sudut bilah kincir air tipe breastshot," *Politeknologi*, vol. 14, no. 3, 2015.

[46] Y. Hara, K. Hara, and T. Hayashi, "Moment of inertia dependence of vertical axis wind Turbines in pulsating winds," *Int. J. Rotating Mach.*, vol. 2012, 2012, doi: 10.1155/2012/910940.

[47] C. Tang, "Analysis and Modelling of the Effects of Inertia and Parameter Errors on Wind Turbine Output Power," *Master Thesis*, 2009.

[48] J. B. S. Kalluvila and B. Sreejith, "Numerical and experimental study on a modified Savonius rotor with guide blades," *Int. J. Green Energy*, vol. 15, no. 12, pp. 744–757, 2018, doi: 10.1080/15435075.2018.1529574.

[49] M. Idris *et al.*, "Water flow simulation in a pelton turbine bucket with variable bucket dimensions using computational fluid dynamic," *JTTM J. Terap. Tek. Mesin*, vol. 4, no. 2, pp. 207–214, 2023, doi: 10.37373/jttm.v4i2.633.

[50] T. J. Erinle, S. O. Ejiko, and D. H. Oladebeye, "Design of Micro Hydro Turbine for Domestic Energy Generation," *Iarjset*, vol. 7, no. 4, pp. 85–93, 2020, doi: 10.17148/iarjset.2020.7414.

[51] N. Acharya, C. G. Kim, B. Thapa, and Y. H. Lee, "Numerical analysis and performance enhancement of a cross-flow hydro turbine," *Renew. Energy*, vol. 80, pp. 819–826, 2015, doi: 10.1016/j.renene.2015.01.064.

[52] V. Sammartano, G. Morreale, M. Sinagra, and T. Tucciarelli, "Numerical and experimental investigation of a cross-flow water turbine," *J. Hydraul. Res.*, vol. 54, no. 3, pp. 321–331, 2016, doi: 10.1080/00221686.2016.1147500.

[53] S. C M and V. Madav, "Numerical and experimental investigation of modified V-shaped turbine blades for hydrokinetic energy generation," *Renew. Energy*, vol. 177, pp. 1170–1197, 2021, doi: 10.1016/j.renene.2021.05.086.

[54] C. M. Shashikumar, V. Hindasageri, and V. Madav, "CFD investigation of unsteady three-dimensional savonius hydrokinetic turbine in irrigation channel with varying positions for hydro power application," *AIP Conf. Proc.*, vol. 2316, 2021, doi: 10.1063/5.0036472.

[55] W. C. Schleicher, J. D. Riglin, and A. Oztekin, "Numerical characterization of a preliminary portable micro-hydrokinetic turbine rotor design," *Renew. Energy*, vol. 76, pp. 234–241, 2015, doi: 10.1016/j.renene.2014.11.032.

[56] I. F. S. dos Santos, R. G. R. Camacho, and G. L. Tiago Filho, "Study of the wake characteristics and turbines configuration of a hydrokinetic farm in an Amazonian river using experimental data and CFD tools," *J. Clean. Prod.*, vol. 299, p. 126881, 2021, doi: 10.1016/j.jclepro.2021.126881.

[57] S. C M, R. Honnasiddaiah, V. Hindasageri, and V. Madav, "Experimental and numerical investigation of novel V-shaped rotor for hydropower utilization," *Ocean Eng.*, vol. 224, no. April 2020, p. 108689, 2021, doi: 10.1016/j.oceaneng.2021.108689.

[58] A. Hamad, S. M. A. Aftab, and K. A. Ahmad, "Reducing Flow Separation in T-Junction Pipe Using Vortex.pdf," *J. Adv. Res. Fluid Mech. Therm. Sci.*, vol. 1, no. 1, pp. 36–46, 2018.

[59] S. Shoeibi, N. Rahbar, A. A. Esfahlani, and H. Kargarsharifabad, "Energy matrices, exergoeconomic and enviroeconomic analysis of air-cooled and water-cooled solar still: Experimental investigation and numerical simulation," *Renew. Energy*, vol. 171, pp. 227–244, 2021, doi: 10.1016/j.renene.2021.02.081.

[60] C. Gnanavel, R. Saravanan, and M. Chandrasekaran, "CFD analysis of solar still with PCM," *Mater. Today Proc.*, vol. 37, no. Part 2, pp. 694–700, 2020, doi: 10.1016/j.matpr.2020.05.638.

[61] A. H. Alami and H. Bilal, "Experimental Evaluation of a Buoyancy Driven Energy Storage Device," *Adv. Mater. Res.*, vol. 816–817, pp. 887–891, 2013, doi: 10.4028/www.scientific.net/AMR.816-817.887.

[62] J. N. Fernando and D. E. Rival, "Characterizing the influence of upstream obstacles on very low head water-turbine performance," *J. Hydraul. Res.*, vol. 52, no. 5, pp. 644–652, 2014, doi: 10.1080/00221686.2014.917809.

Dan Mugisidi - Effect of buoyancy force on buoyancy waterwheel efficiency using numerical flow simulation

by Layanan Perpustakaan UHAMKA

Submission date: 14-Mar-2024 11:00AM (UTC+0700)
Submission ID: 2320011332
File name: 976-Article_Text-7488-3-10-20240303.pdf (1.22M)
Word count: 6247
Character count: 32398

ISSN 2087-3336 (Print) | 2721-4729 (Online)

TEKNOSAINS: Jurnal Sains, Teknologi dan Informatika

Vol 11, No. 2, July 2024, page. 209-221

http://jurnal.sttmcileungsi.ac.id/index.php/tekno

DOI: 10.37373

Effect of buoyancy force on buoyancy waterwheel efficiency using numerical flow simulation

Fadhlurrahman Zaki, Dan Mugisidi*

* Mechanical Engineering, Faculty of Industrial Technology and Information Technology, Muhammadiyah University Prof. Dr. Hamka, Indonesia, 13830. Jl. Tanah Merdeka No.6, RT.10/RW.5 13830 Region of Jakarta, Indonesia

*✉ dan.mugisidi@uhamka.ac.id

Submitted: 30/12/2023 Revised: 15/01/2024 Accepted: 07/02/2024

ABSTRACT

In this work, the performance of a buoyant waterwheel to produce hydrokinetic power is investigated through analytical theory and computational fluid dynamics simulation. The impact of the buoyancy wheel is investigated by establishing the performance parameters through the use of a moving mesh approach and a realizable k-ε turbulence model. Transient simulation is required to comprehend the flow of physical processes. Using moving mesh as a transient methodology of the buoyancy waterwheel, numerical flow simulations and theoretical analytical methods are used in this study to assess the effect of buoyant force generated on the performance of the buoyancy wheel. The buoyancy waterwheel that will be put to the test has eight straight blades and a diameter of one meter. The pinwheel force and torque created in the numerical flow simulation (CFD) are 414.96 N and 207.48 Nm, respectively, whereas in the theoretical calculation, they are 449.06 N and 224.53 Nm, according to the research findings. It is possible to compute the buoyancy wheel's power output and efficiency mathematically, yielding values of 1619.35 W and 68.07%. The buoyancy wheel's power output and efficiency, as determined by numerical flow simulation, are 1495.95 W and 62.88%, respectively. Based on theoretical and CFD study results, the buoyancy wheel generates a standard deviation of 7.62%. Thus, for the buoyancy wheel, a temporary method that takes advantage of the moving mesh characteristic is advised. This method can also be applied as a future alternative energy source for the Piko hydro turbine.

Keywords: Renewable energy; waterwheel; CFD; moving mesh; hydropower

1. INTRODUCTION

Year after year, Indonesia's requirement for electrical energy keeps growing [1]. Because of the depletion of non-renewable natural resources, research is being done on the potential of renewable energy to provide electricity [2],[3]. Indonesia create renewable energy sources like hydro energy because it is a tropical nation [4],[5], wind energy [6]–[10], geothermal energy [11], biogas energy [12], and biomass energy [13]. Hydropower is regarded as a clean, sustainable energy source with enormous growth potential [14]. By 2025, the Indonesian government wants to use 23% renewable energy, particularly in the country's outlying regions [15]. Pico hydro is the term for water energy, which falls under the lowest size category and has a maximum production of 5 kW [16]. The process of operating a pico hydro water turbine involves using the turbine's rotation to generate mechanical energy [17]. An electric generator uses a revolving turbine to transform mechanical energy into electrical energy. Numerous varieties of hydraulic turbines exist: Reaction turbines (like Francis and Kaplan) employ water pressure, impulse turbines (like Pelton, Turgo, and Banki) use water kinetic energy, and gravity turbines (like water wheels and Archimedes screws) rely mostly on water weight [18],[19].

A great deal of research has been done to enhance turbine performance to solve this issue. William and Samson believe that a pico hydro turbine would be a wise decision [20], the feasibility analysis of self-sufficient electricity production for outlying areas. The effectiveness of waterwheels in connection to the ratio of immersion radius to paddle count was examined by Tevata and Inprasit. Their research indicates a significant relationship between the torque load of a waterwheel running at maximum power and the dipping radius ratio [21]. As stated by Quaranta [22]–[24], The efficacy of the breastshot waterwheel can be increased by numerically and experimentally altering the overshot waterwheel's geometry with a circular wall encircling the wheel. Warjito also examined the quantity of distinct buckets to evaluate the flow field's performance and quality. The efficiency of water wheels is expected to be significantly impacted by the design of the radial blades [25]. Next, Adanta assessed Warjito's proposal [25]. Each wheel's moment of inertia is determined using the CFD approach with 6-DoF characteristics. Thus, 20 blades get the best results, but 8 blades yield the most consistent results [26].

In the realm of renewable energy, the combination of buoyancy and water wheel is particularly promising for hydroelectric power plants [27]. In fluid mechanics, the upward force a fluid exerts on a submerged object is known as the buoyant force [28]. Archimedes' principle states that this force is equal to the weight of the fluid displaced by the submerged item [29]. This idea is particularly clear in fluids like water, where items float or have a reduced effective weight because buoyant force opposes gravity [30]. A submerged object's buoyant force is produced by the pressure differential between its top and bottom, with higher pressure at the bottom providing an upward push [31]. This means that new avenues for optimizing energy extraction from dynamic water settings are made possible by the strategic interaction of buoyancy forces with water wheels [32].

Compared to experimental and analytical techniques, CFD methods can depict the flow field in greater detail [33]. Moving Mesh was selected for the temporary method since it uses less processing resources and is frequently employed by researchers [34]–[36]. Using moving mesh as a transient methodology for buoyancy wheels, computational fluid dynamics (CFD) and theoretical analytical methods are used in this study to estimate the power and efficiency produced by buoyancy wheels.

2. METHOD

2.1. Governing equation

The following is equation (1) of continuity for incompressible fluids based on the rule of conservation of mass [37].

$$\frac{\partial \rho}{\partial t}+\frac{\partial \rho U_i}{\partial x_i}=0 \tag{1}$$

The Navier-Stokes momentum equation, equation (2), can be computed as follows by applying the momentum conservation law:

$$\frac{\partial \rho U_i}{\partial t}+\frac{\partial \rho U_i U_j}{\partial x_j}=\frac{\partial \rho}{\partial x_i}+\frac{\partial}{\partial x_i}\left[(\mu+\mu_t)\left(\frac{\partial U_i}{\partial x_j}+\frac{\partial U_j}{\partial x_i}\right)\right] \tag{2}$$

where ρ represents the density of water, Ui the speed, t the time, and coordinates x_i and x_j, in addition to turbulence and molecular viscosity by μ and μ_t respectively.

2.1.1. VOF method

The distance between the free liquid level and the bed bottom in the multiphase flow module is represented by the VOF model, which investigates the gas-liquid interface in unpressurized flow as a two-phase flow problem. It is defined that the Navier-Stoke equations apply to uniformly incompressible fluids [38]:

$$\nabla \cdot \bar{u}=0 \tag{3}$$

$$\frac{\partial \bar{u}}{\partial \mathrm{t}}+(\bar{u}\cdot\nabla)\bar{u}=-\frac{1}{\rho}\nabla\bar{p}+\mu\nabla^2\bar{u}+\rho g \tag{4}$$

Where $\bar{u}$ denotes the speed, μ is the dynamic viscosity coefficient, $\bar{p}$ denotes pressure, ρ is the density of the fluid, and g represents the acceleration due to gravity. The location of the gas-liquid interface can be found by solving the volume fraction of each phase as follows:

$$\frac{\partial \alpha_q}{\partial t} + \frac{\partial \alpha_q \bar{u}_i}{\partial x_i} + \frac{\partial \alpha_q \bar{u}_j}{\partial x_j} + \frac{\partial \alpha_q \bar{u}_w}{\partial x_w} = 0 \quad (5)$$

Where α_q is the volume fraction of water from each grid? When α_q = 1, there is the same amount of water in the grid. There is no liquid in the grid if α_q = 0. when the air-water-free is in the range of 0 to 1. After determining the volume fraction of water α_q, hence the gas volume fraction α_p = 1 - α_q. Equation (6) determines the volume fraction, which is used to model the density and dynamic viscosity coefficients [39]:

$$\mu = \alpha_q \mu_q + (1 - \alpha_q)\mu_p \quad (6)$$

$$\rho = \alpha_q \rho_q + (1 - \alpha_q)\rho_p \quad (7)$$

2.1.2. k- ε turbulence model

An enhanced method is employed to compute the turbulent viscosity in the acceptable k-ε model. Using the proper transport equation of the fluctuating components' vortex strength, one can construct the dissipation rate equation. It is considered the k model is admissibly more accurate than the k-ε model in forecast the dissipation rate distribution of flat and spherical jets. Furthermore, plausible k-ε models allow for better predictions of boundary layer parameters at large pressure gradients and in separated and revolving flows [40]. The model's transport equations are each written as [40].

$$\frac{\partial}{\partial t}(\rho k) + \frac{\partial}{\partial t}(\rho k\, u_i) = \frac{\partial}{\partial x_i}\left[\left(\mu + \frac{u_t}{\sigma_k}\right)\frac{\sigma_k}{\sigma_{xj}}\right] + G_k + G_b - \rho\varepsilon - Y_M + S_k \quad (8)$$

$$\frac{\partial}{\partial t}(\rho \varepsilon) + \frac{\partial}{\partial t}(\rho \varepsilon\, u_i) = \frac{\partial}{\partial x_j}\left[\left(\mu + \frac{u_t}{\sigma_k}\right)\frac{\sigma_\varepsilon}{\sigma_{xj}}\right] + C_{1\varepsilon}\frac{\varepsilon}{k}(G_k + G_{3\varepsilon} + G_b) - C_{2\varepsilon}\rho\frac{\varepsilon^2}{k} + S_\varepsilon \quad (9)$$

2.2. Model matematika

A full-size flow buoyancy wheel consists of an eight-bladed, straight, basic wheel. Diagonal propellers are being created to perform better in future studies. The rational area and flow area of the waterwheel are mostly included in a 3D model that is built using CAD software. The water wheel measures 0.16 meters in width (b), 1 meter in outer diameter (D), 0.3 meters in hub diameter (d), 0.0018 meters in thickness (t) for the wheel blades, and 0.02 meters inside clearance. This optimizes the energy in motion. Waterwheels are made of aluminum type 6061, which has a density of 2700 kg/m^3. The general design specifications are shown in Table 1. Figure 1 shows the test model design for the buoyancy wheel operation.

Table 1. Buoyancy wheel design parameters

Design parameters	Value
Rated output power, P_{rated} (kW)	1.3
The outer radius of the wheel, R (m)	0.5
Waterwheel width, b (m)	0.16
Blade dimensions (m) (Length x Width x Thickness)	0.00345 x 0.15 x 0.0018
Blade shape	Rectangle

For the analytical design of the water wheel, the researchers provided technical background. Cornelis defines the power output of a water wheel as Equation (10) [41]:

$$P_{out} = \tau \cdot \omega \quad (10)$$

Where T shows the torque and angular speed of the water wheel. Plotkin describes the resulting torque in Equation (11) [42]:

$$\tau = F \cdot \frac{D}{2} \tag{11}$$

Equation (10) added to Equation (11) will produce equation (12) [43]:

$$P_{out} = F \cdot \omega \cdot \frac{D}{2} \tag{12}$$

Floating water wheels are designed to operate in both air and water zones, as seen in Figure 2. Figure 2 shows a floating water wheel with a free-body diagram representing the ambient conditions and working forces. The buoyant force of the air in the water zone and the gravity of the water in the air zone are what cause this water wheel to circle. The water wheel is turned by the torque created by the water-filled bucket falling through the air [24]. There is more air trapped in bucket 4 than water when it reaches bucket 5 in position. Because of this, the combined bucket's density is less than that of water, creating a buoyant force (Fb). This process is repeated for all eight buckets, leaving four in the various work zones with water and four with air inside [44]. The combined weight of the water and the air's lifting force generates the torque and power that the water wheel produces as it rotates [45]. The following equations (14)–(21) can be used to compute the force applied to the floating water wheel.

$$d_{shaft} = \sqrt[3]{\frac{16 \cdot \tau_{max} \cdot FS}{\pi \cdot \sigma_{yield}}} \tag{13}$$

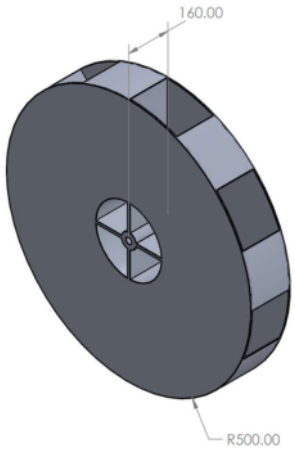

Figure 1. 3D model design of the buoyancy wheel

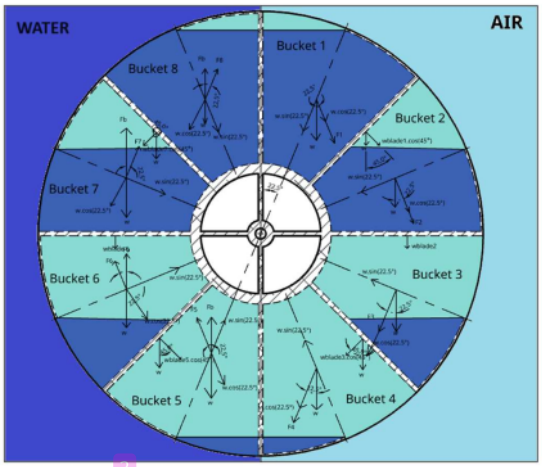

Figure 2. Free body diagram of the buoyancy wheel

The buoyancy wheel is designed to work in both air and water zones, as seen in Figure 2. Figure 2 shows a buoyancy wheel with a free-body diagram representing the working forces and ambient conditions. The buoyant force of the air in the water zone and the gravity of the water in the air zone are what cause this water wheel to circle. The water wheel is turned by the torque created by the water-filled bucket falling through the air [24]. There is more air trapped in bucket 4 than water when it reaches bucket 5 in position. Because of this, the combined bucket's density is less than that of water, creating a buoyant force (Fb). This process is repeated for all eight buckets, leaving four in the various work zones with water and four with air inside [44]. The combined weight of the water and the air's lifting force generates the torque and power that the water wheel produces as it rotates [45]. The force exerted on the buoyancy wheel can be calculated using equations (14)-(21) below.

$$F_1 = w \cdot \cos\theta = (m_{air} \cdot \cos 22.5° + m_{blade} \cdot \cos 45°) \cdot g \tag{14}$$

$$F_2 = w \cdot \cos\theta = (m_{air} \cdot \cos 22.5° + m_{blade}) \cdot g \quad (15)$$

$$F_3 = w \cdot \cos\theta = (m_{air} \cdot \cos 22.5° + m_{blade} \cdot \cos 45°) \cdot g \quad (16)$$

$$F_4 = w \cdot \cos\theta = (m_{water} \cdot \cos 45°) \cdot g \quad (17)$$

$$F_5 = \rho_{water} \cdot g \cdot V_{bucket} \cdot \cos 22.5° - \rho_{material} \cdot g \cdot V_{blade} \cdot \cos 45° \quad (18)$$

$$F_6 = \rho_{water} \cdot g \cdot V_{bucket} \cdot \cos 22.5° - \rho_{material} \cdot g \cdot V_{blade} \quad (19)$$

$$F_7 = \rho_{water} \cdot g \cdot V_{bucket} \cdot \cos 22.5° - \rho_{material} \cdot g \cdot V_{blade} \cdot \cos 45° \quad (20)$$

$$F_8 = \rho_{water} \cdot g \cdot V_{bucket} \cdot \cos 22.5° \quad (21)$$

To making the moment of inertia calculation easier, it is assumed that the water wheel is straight. At that point, the waterwheel bucket can be roughly modeled as a solid cylinder [46]. where m is the water wheel's mass and r is its outer radius. Therefore, using equation (22) the buoyancy wheel's inertia can be computed as follows [47]:

$$I = \frac{1}{2} \cdot m \cdot r^2 = \frac{1}{2} \rho \cdot V \cdot r^2 \quad (22)$$

Equations (23) and (24) are used to determine the angular velocity (ω) and wheel speed respectively [48],[49]:

$$\omega = \frac{2\pi \cdot N}{60} \quad (23)$$

$$v = \omega \cdot r \quad (24)$$

where N is the turbine revolutions per minute. Equation (25) is used to calculate the input power (P_{in}) [50]:

$$P_{in} = \rho \cdot g \cdot Q \cdot H \quad (25)$$

Where Q is discharge, H is head, ρ is water density and g is acceleration caused by gravity. Equation (26) is the ratio of the power available at the shaft (P_{out}) to input power (P_{in}) called hydraulic efficiency (η) [51]:

$$\eta = \frac{P_{out}}{P_{in}} \quad (26)$$

2.3. Boundary conditions and simulation setup

As seen in Figure 3, boundary conditions (BC) define a rotating domain and a static domain. In the rotational domain, the water wheel is set up as a wall-type BC, and the k-ε turbulence model used in this simulation is derived from earlier studies on picohydro water turbines conducted by different researchers [52]. Since this simulation is multiphase, the rotating domain is where fluids like air and water are defined [53]. Both have a zero-speed initialization. Water and air were once half-domains that were both stationary and rotating. Domain gravity is 9.81 m/s about the suitable coordinate system [54]. The right-hand rule states that throughout domain movement, the domain will spin at a constant speed of 69 revolutions per minute. Numerous boundary conditions (BCs) are provided, such as zero outlet pressure, one meter per second (m/s) input velocity for air 0.121 m^3/s for water utilizing Qin, and non-slip wall boundary conditions. In a similar vein, it is believed that the domain's surface facing the atmosphere serves as a symmetric border condition. Inner and outer interfaces link the spinning and stationary domains [49].

P-V coupling is handled by the SIMPLE scheme, momentum is handled by the Body Force Weighted for Pressure scheme, and spatial discretization is handled by the 2nd-order upwind scheme [55]. The convergence criteria of the turbulence equations, momentum, and continuity requirements are satisfied by the values 1×10^{-4} [56]. An implicit scheme is used to calculate the volume fraction. To achieve a balance between accuracy and efficiency, the simulation time for each time step is set to 20 iterations. A time step size of 0.025s was chosen for transient simulation.

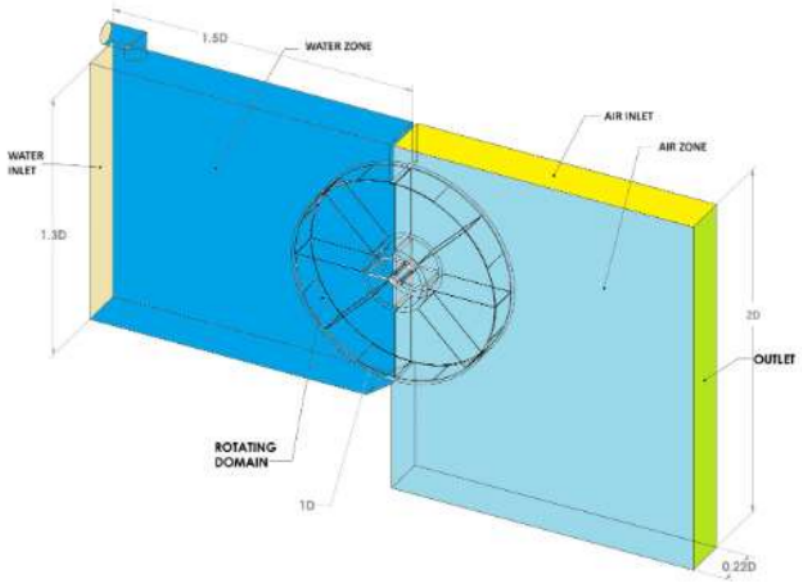

Figure 3. Boundary conditions for the buoyancy wheel simulation setup.

2.4. Grid independency test

A three-dimensional (3D) model of the water wheel and the surrounding flow field domain is created to compare with the analytical results. The characteristics and performance of the buoyancy wheel were analyzed using ANSYS 18.1. The wheel and fluid domains use tetrahedral meshes due to the complexity of the system [57]. The goal of the Grid Independence Test is to ensure that the results do not depend on additional grid refinements [58]. The grid Independence Test is a technique to reduce computing time and costs by avoiding using the best grid. The test-independent grid can be said to have converged if the error is less than 1% [59], [60]. Numerical analysis was performed and five grids with varying degrees of fineness were created in this study. By plotting torque results against the number of elements in a particular mesh type, the Grid Independence Test shows that grid size significantly influences turbine torque performance. From Figure 4 it can be seen that a mesh with 0.57 million elements produces almost the same power results as a mesh with 0.86 million elements and the mesh distribution used is shown in Figure 5. Therefore, to get accurate results with less time and computational costs in this study, a mesh with 0.57 million elements was used for this simulation.

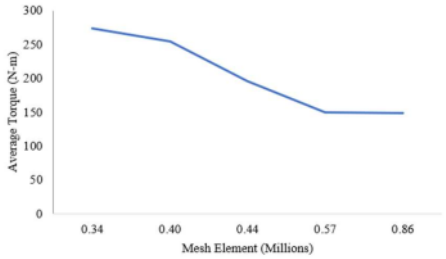

Figure 4. Effect of grid refinement on the torque produced by the turbine

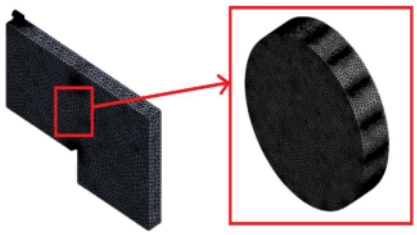

Figure 5. Visualization of 0.57 million mesh elements

3. RESULTS AND DISCUSSION

3.1. Theoretical analysis results

First estimates of the water resources at the mechanical engineering laboratory were used to build the buoyancy wheel, which has a 2 m head and a 0.121 m^3/s water output. Equations (14)–(17) are used to determine the buoyancy force components while equations (18)–(21) are used to calculate the gravity components of the buoyancy wheel (Figure 2). Table 2 and Figure 6 exhibit the style analysis's findings.

Table 2. Analysis of the forces acting on the buoyancy wheel

No. Bucket	Force (N)
Bucket 1	115.98
Bucket 2	91.33
Bucket 3	32.39
Bucket 4	5.02
Bucket 5	4.26
Bucket 6	26.46
Bucket 7	86.26
Bucket 8	87.37
Total	449.06

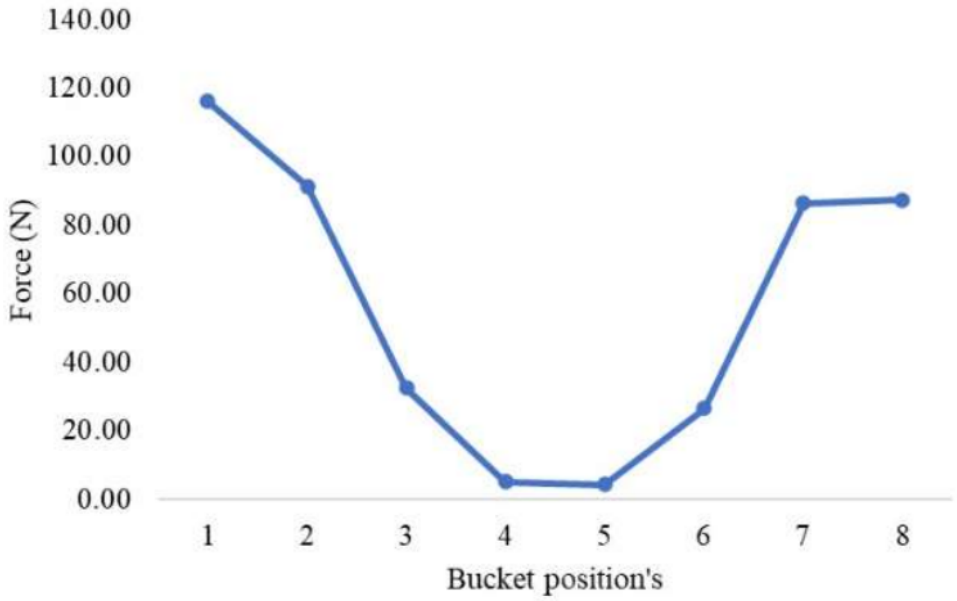

Figure 6. Forces acting on a floating waterwheel.

Equation (11) is used to compute the buoyancy wheel's torque component, which equals 224.53 N-m when the force produced by the buoyancy wheel's radius is multiplied. Equations (22), (23), (13), and (24) are used to compute the moment of inertia (I), angular velocity (ω), shaft diameter (do), and buoyancy wheel speed (v) from the buoyancy wheel design. Table 3 displays the findings of the parameter data.

Table 3. Several parameters that work on the buoyancy wheel

Parameters	Value
Moment of Inertia, I ($kg.m^2$)	4.31
Rotation speed, ω, (rad/s)	7.21
Shaft diameter, d_o (mm)	30
Buoyancy wheel speed, v (m/s)	3.61

3.2. CFD analysis results

3.2.1. Effect of buoyancy force on buoyancy wheel performance

The water volume fraction in the eight buckets can function because of the difference in water height between the water and air zones, according to the simulation findings shown in Figure 7. The buoyancy wheel is operated by the force mechanisms of buoyancy and gravity. The findings demonstrated that as the amount of water held in the bucket rose, its buoyancy increased as well. The buoyancy wheel's air and water fluids have different specific gravities of 0.00123 and 0.998, respectively, which causes an increase in buoyancy force. When the air-filled bucket starts to enter the water zone, there is a difference in specific gravity that causes a buoyant force that pushes the bucket upward and causes the wheel to rotate. Every object submerged in a fluid, whether fully or partially, will experience an upward buoyant force equal to the weight of the fluid displaced by the object, according to Archimedes' Law [61].

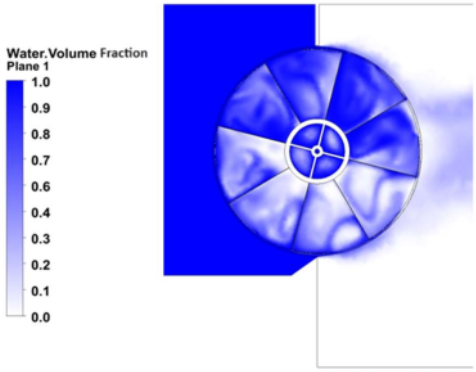

Figure 7. The volume fraction of water working on the buoyancy wheel.

3.2.2. Speed contours on the buoyancy wheel

Figure 8 further demonstrates that, throughout the majority of the domain width, the fluid velocity in the upstream region is constant. The downstream velocity profile, which also demonstrates that the fluid velocity is zero at the wall but changes rapidly across the width of the fluid domain due to the rotational motion of the turbine, indicates that the fluid velocity behind the turbine is lower due to the development of the wake region and the extraction of turbine kinetic energy from water molecules. After the water's kinetic energy is extracted by the turbine's buoyancy, the water's kinetic energy is diminished downstream, and the mechanical energy is accessible at the turbine shaft.

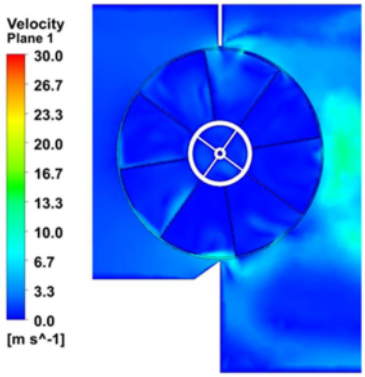

Figure 8. Buoyancy wheel speed contour

Simultaneously, a high-velocity zone appears at the advancing blade tip, indicating the dynamic nature of fluid dynamics during the simulation. Contour plots effectively highlight these variations, with red representing high speeds and blue depicting low speeds. This visual representation allows a clear

understanding of fluid behavior during turbine bucket rotation. Figure 8 shows the findings of the distribution of water flow velocity from each waterwheel bucket. With a maximum value of 30 m/s, the red color shows the area with the highest flow speed, while the light blue color shows the area with the lowest water flow speed, namely 3.3 m/s. The resulting buoyancy wheel speed is 3.6 m/s during this simulation.

3.3. Buoyancy wheel performance validation

It is possible to comprehend buoyancy wheel performance efficiency by employing numerical flow simulation analysis in conjunction with theoretical study. While computational analysis can offer a more comprehensive understanding of the factors influencing buoyancy wheel efficiency, numerical flow simulation analysis can offer a more accurate representation of the water flow surrounding a buoyancy wheel [62]. As demonstrated in Table 4, these two analytic methods can be used concurrently for more accurate findings. Equation (25) yields an input power (Pin) of 2378.99 W. In addition, 414.96 N of force and 207.48 N-m of torque are produced in the numerical flow simulation. The buoyancy wheel's performance efficiency can be computed using equation (26). It was discovered that the power generated by the numerical flow simulation analysis was 1495.95 W, while the power generated by the theoretical analysis utilizing equation (10) was 1619.35 W. In the numerical flow simulation, the buoyancy wheel produced an efficiency of 62.88%, but in the theoretical study, it was 68.07%. These findings show that the buoyancy wheel's performance created a 7.62% variance.

Table 4. Performance parameters on the buoyancy wheel

Parameter	Theoretical Results	CFD	Diff.
Power output, P_{out} (W)	1619.35	1495.95	0.0762
Eff. (%)	68.07%	62.88%	7.62%

4. SIMPULAN

Indonesia's annual demand for electrical energy is still rising. Research is being done on renewable energy as a source of energy for producing power because non-renewable natural resources are becoming scarce. It is appropriate to use CFD techniques to look into physical flow phenomena in the research of buoyancy wheels to completely comprehend the energy conversion process. Moving meshes are a common way for CFD algorithms to provide the boundary conditions for transient approximations for rotating case objects. Thus, using theoretical analysis techniques and CFD with moving mesh as a transient methodology for the buoyancy wheel, the goal of this research is to ascertain the impact of the ensuing buoyant force on the buoyancy wheel's performance. The force and torque generated by numerical calculations and simulations are 449.06 N and 224.53 Nm, respectively; 414.96 N and 207.48 Nm, according to the research findings. Additionally, the power generated by the numerical simulation and theoretical analysis is 1495.95 W and 1619.35 W, respectively. The buoyancy wheel generates an efficiency of 68.07% and 62.88%, yielding a 7.62% variance.

ACKNOWLEDGEMENT

Thank you to LEMLITBANG UHAMKA for funding this internal research with contract number 53/F.03.07/2022 and the Faculty of Industrial Technology and Information Technology (FTII) UHAMKA for facilitating research facilities and infrastructure.

REFERENCE

[1] D. Adanta, R. Fattah, and N. M. Muhammad, "COMPARISON OF STANDARD k-ε AND SST k-ωTURBULENCE MODEL FOR.pdf," *Mech. Sci. Eng.*, vol. 7, no. 2, pp. 39–44, 2020.

[2] P. Sritram and R. Suntivarakorn, "Comparative Study of Small Hydropower Turbine Efficiency at Low Head Water," *Energy Procedia*, vol. 138, pp. 646–650, 2017, doi: 10.1016/j.egypro.2017.10.181.

[3] O. D. Monsalve-Cifuentes, J. Graciano-Uribe, and D. A. H. Zuluaga, "Numerical Simulation of

a Propeller-Type Turbine for In-Pipe Installation," *J. Adv. Res. Fluid Mech. Therm. Sci.*, vol. 83, no. 1, pp. 1–16, 2021, doi: 10.37934/arfmts.83.1.116.

[4] A. W. Biantoro, I. Iskendar, S. Subekti, and N. H. Bin Muhd Noor, "The Effects of Water Debit and Number of Blades on the Power Generated of Prototype Turbines Propeller as Renewable Electricity," *J. Rekayasa Mesin*, vol. 12, no. 1, p. 203, 2021, doi: 10.21776/ub.jrm.2021.012.01.22.

[5] R. Klar, B. Steidl, and M. Aufleger, "A floating energy storage system based on fabric," *Ocean Eng.*, vol. 165, no. July, pp. 328–335, 2018, doi: 10.1016/j.oceaneng.2018.07.051.

[6] H. Im and B. Kim, "Power Performance Analysis Based on Savonius Wind Turbine Blade Design and Layout Optimization through Rotor Wake Flow Analysis," *Energies*, vol. 15, no. 24, 2022, doi: 10.3390/en15249500.

[7] M. Yusvika, A. Sutaji, A. R. Prabowo, F. Imaduddin, and S. Hadi, "Prediction of the Hydrodynamic Performance of an Elliptical Blade Savonius Turbine using Computational Fluid Dynamics," *IOP Conf. Ser. Mater. Sci. Eng.*, vol. 1096, no. 1, p. 012050, 2021, doi: 10.1088/1757-899x/1096/1/012050.

[8] F. D. Scheaua, "An alternative for wind energy conversion using improved Savonius rotor turbine model," *IOP Conf. Ser. Mater. Sci. Eng.*, vol. 1182, no. 1, p. 012069, 2021, doi: 10.1088/1757-899X/1182/1/012069.

[9] F. Balduzzi, A. Bianchini, R. Maleci, G. Ferrara, and L. Ferrari, "Critical issues in the CFD simulation of Darrieus wind turbines," *Renew. Energy*, vol. 85, pp. 419–435, 2016, doi: 10.1016/j.renene.2015.06.048.

[10] S. Susastro, A. Noerpamoengkas, M. Ulum, and G. Setyono, "Performance Analysis of Wind Power Generation Models Using Oscillating Water Column," *JRST (Jurnal Ris. Sains dan Teknol.*, vol. 4, no. 2, p. 57, 2020, doi: 10.30595/jrst.v4i2.6020.

[11] A. A. Ahmed, M. Assadi, A. Kalantar, T. Sliwa, and A. Sapińska-śliwa, "A Critical Review on the Use of Shallow Geothermal Energy Systems for Heating and Cooling Purposes," *Energies*, vol. 15, no. 12, pp. 1–23, 2022, doi: 10.3390/en15124281.

[12] M. J. B. Kabeyi and O. A. Olanrewaju, "Biogas Production and Applications in the Sustainable Energy Transition," *J. Energy*, vol. 2022, pp. 1–43, 2022, doi: 10.1155/2022/8750221.

[13] M. M. Tun, D. Juchelkova, M. M. Win, A. M. Thu, and T. Puchor, "Biomass energy: An overview of biomass sources, energy potential, and management in Southeast Asian countries," *Resources*, vol. 8, no. 2, 2019, doi: 10.3390/resources8020081.

[14] M. S. Güney and K. Kaygusuz, "Hydrokinetic energy conversion systems: A technology status review," *Renew. Sustain. Energy Rev.*, vol. 14, no. 9, pp. 2996–3004, 2010, doi: 10.1016/j.rser.2010.06.016.

[15] D. Mugisidi, I. N. Fauzi, O. Heriyani, Y. Djeli, E. Aidhilhan, and P. H. Gunawan, "Development of the Dethridge Wheel Blade Shape for Hydropower Generation in Irrigation Canals in Indonesia," *J. Adv. Res. Fluid Mech. Therm. Sci.*, vol. 98, no. 2, pp. 146–156, 2022, doi: 10.37934/arfmts.98.2.146156.

[16] F. B. Darsono, R. D. Widodo, Rusiyanto, and A. Nurdin, "Analysis Of the Effect of Flow Rate and Speed on Four Blade Tubular Water Bulb-Turbine Efficiency Using Numerical Flow Simulation," *J. Adv. Res. Fluid Mech. Therm. Sci.*, vol. 90, no. 2, pp. 1–8, 2022, doi: 10.37934/arfmts.90.2.18.

[17] E. Quaranta, J. P. Perrier, and R. Revelli, "Optimal design process of crossflow Banki turbines: Literature review and novel expeditious equations," *Ocean Eng.*, vol. 257, no. January, p. 111582, 2022, doi: 10.1016/j.oceaneng.2022.111582.

[18] E. Quaranta and R. Revelli, "Gravity water wheels as a micro hydropower energy source: A review based on historic data, design methods, efficiencies and modern optimizations," *Renew. Sustain. Energy Rev.*, vol. 97, no. November 2017, pp. 414–427, 2018, doi: 10.1016/j.rser.2018.08.033.

[19] D. K. Okot, "Review of small hydropower technology," *Renew. Sustain. Energy Rev.*, vol. 26, pp. 515–520, 2013, doi: 10.1016/j.rser.2013.05.006.

[20] A. A. Williams and R. Simpson, "Pico hydro - Reducing technical risks for rural electrification," *Renew. Energy*, vol. 34, no. 8, pp. 1986–1991, 2009, doi: 10.1016/j.renene.2008.12.011.

[21] A. Tevata and C. Inprasit, "The effect of paddle number and immersed radius ratio on water wheel performance," *Energy Procedia*, vol. 9, pp. 359–365, 2011, doi: 10.1016/j.egypro.2011.09.039.

[22] E. Quaranta and R. Revelli, "Hydraulic Behavior and Performance of Breastshot Water Wheels for Different Numbers of Blades," *J. Hydraul. Eng.*, vol. 143, no. 1, pp. 1–10, 2017, doi: 10.1061/(asce)hy.1943-7900.0001229.

[23] E. Quaranta and R. Revelli, "CFD simulations to optimize the blade design of water wheels," *Drink. Water Eng. Sci.*, vol. 10, no. 1, pp. 27–32, 2017, doi: 10.5194/dwes-10-27-2017.

[24] E. Quaranta and R. Revelli, "Output power and power losses estimation for an overshot water wheel," *Renew. Energy*, vol. 83, pp. 979–987, 2015, doi: 10.1016/j.renene.2015.05.018.

[25] Wariito, D. Adanta, S. A. Arifianto, S. B. Nasution, and Budiarso, "Effect of Blades Number on Undershot Waterwheel Performance with Variable Inlet Velocity," *Proc. - 2018 4th Int. Conf. Sci. Technol. ICST 2018*, no. 4749, pp. 1–6, 2018, doi: 10.1109/ICSTC.2018.8528714.

[26] Warjito, D. Adanta, Budiarso, and A. P. Prakoso, "The effect of bucketnumber on breastshot waterwheel performance," *IOP Conf. Ser. Earth Environ. Sci.*, vol. 105, no. 1, 2018, doi: 10.1088/1755-1315/105/1/012031.

[27] C. M. Wang, T. Utsunomiya, S. C. Wee, and Y. S. Choo, "Research on floating wind turbines: A literature survey," *IES J. Part A Civ. Struct. Eng.*, vol. 3, no. 4, pp. 267–277, 2010, doi: 10.1080/19373260.2010.517395.

[28] Mr. Shivakumar M, "The Law of Buoyancy Force," *Int. J. Eng. Res.*, vol. V5, no. 02, pp. 183–185, 2016, doi: 10.17577/ijertv5is020264.

[29] A. H. Alami, *General Concepts BT - Mechanical Energy Storage for Renewable and Sustainable Energy Resources*. 2020. [Online]. Available: http://www.springer.com/series/15883

[30] A. Nergaard, N. Architect, and P. Engineer, "The Magic of Buoyancy and Hydrostatics – Buoyancy and Effective Forces," *Mod. Appl. Sci.*, vol. 11, no. 12, p. 77, 2017, doi: 10.5539/mas.v11n12p77.

[31] T. Ozturk and A. Demirbas, "Electricity generation using water lifting force," *Energy Explor. Exploit.*, vol. 24, no. 4–5, pp. 285–296, 2006, doi: 10.1260/014459806779398794.

[32] A. H. Alami, "Analytical and experimental evaluation of energy storage using work of buoyancy force," *J. Renew. Sustain. Energy*, vol. 6, no. 1, 2014, doi: 10.1063/1.4866036.

[33] T. Kolšek, J. Duhovnik, and A. Bergant, "Simulation of unsteady flow and runner rotation during shut-down of an axial water turbine," *J. Hydraul. Res.*, vol. 44, no. 1, pp. 129–137, 2006, doi: 10.1080/00221686.2006.9521668.

[34] C. D. Widiawaty *et al.*, "Optimization of inverse-Prandtl of Dissipation in standard k-ε Turbulence Model for Predicting Flow Field of Crossflow Turbine," *CFD Lett.*, vol. 14, no. 1, pp. 112–127, 2022, doi: 10.37934/cfdl.14.1.112127.

[35] R. Pienika, G. Usera, and H. M. Ramos, "Simulation of a hydrostatic pressure machine with caffa3d solver: Numerical model characterization and evaluation," *Water (Switzerland)*, vol. 12, no. 9, 2020, doi: 10.3390/w12092419.

[36] A. G. P. Narrain, *Low head hydropower for local energy solutions*. 2017. doi: 10.1201/9781351182720.

[37] W. Feng, Y. Zheng, A. Yu, and Q. Tang, "Experimental and Numerical Analysis of the Clearance Effects between Blades and Hub in a Water Wheel Used for Power Generation," *Water*, vol. 14, no. 22, p. 3640, 2022, doi: 10.3390/w14223640.

[38] T. Bikmukhametov, "CFD Simulations of Multiphase Flows with Particles," Norwegian

University of Science and Technology, 2016. [Online]. Available: https://brage.bibsys.no/xmlui/handle/11250/2405984

[39] O. Elshawarby, "Computational Fluid Dynamics of Multiphase Flow Using ANSYS Fluent," 2021.

[40] H. Kheirkhah Gildeh, A. Mohammadian, I. Nistor, H. Qiblawey, and X. Yan, "CFD modeling and analysis of the behavior of 30° and 45° inclined dense jets - New numerical insights," *J. Appl. Water Eng. Res.*, vol. 4, no. 2, pp. 112–127, 2016, doi: 10.1080/23249676.2015.1090351.

[41] S. Cornelis, "Parametric study of the performance of an impulse-type turbine with CFD," 2015.

[42] K. V. Poletkin, "Calculation of magnetic force and torque between two arbitrarily oriented circular filaments using Kalantarov–Zeitlin's method," *Int. J. Mech. Sci.*, vol. 220, pp. 1–39, 2022, doi: 10.1016/j.ijmecsci.2022.107159.

[43] Z. Nurfadilah, D. Mugisidi, A. R. S. Pohan, and O. Heriyani, "Pengaruh Kincir Tertutup Terhadap Efisiensi dan Rugi-rugi," *Rekayasa Energi Manufaktur) J.* |, vol. 8, no. 1, pp. 2528–3723, 2023, [Online]. Available: http://doi.org/10.21070/rem.v8i1.1670

[44] E. Prihastuty and H. D. Harsono, "Perancangan Kincir Air Undershot Sebagai Penggerak Awal Pompa," *Mestro*, pp. 1–7, 2019, [Online]. Available: http://jurnal.untagcirebon.ac.id/index.php/mestro/article/view/27

[45] A. Syuriadi and A. Nidhar, "Pengujian variasi jumlah dan sudut bilah kincir air tipe breastshot," *Politeknologi*, vol. 14, no. 3, 2015.

[46] Y. Hara, K. Hara, and T. Hayashi, "Moment of inertia dependence of vertical axis wind Turbines in pulsating winds," *Int. J. Rotating Mach.*, vol. 2012, 2012, doi: 10.1155/2012/910940.

[47] C. Tang, "Analysis and Modelling of the Effects of Inertia and Parameter Errors on Wind Turbine Output Power," *Master Thesis*, 2009.

[48] J. B. S. Kalluvila and B. Sreejith, "Numerical and experimental study on a modified Savonius rotor with guide blades," *Int. J. Green Energy*, vol. 15, no. 12, pp. 744–757, 2018, doi: 10.1080/15435075.2018.1529574.

[49] M. Idris *et al.*, "Water flow simulation in a pelton turbine bucket with variable bucket dimensions using computational fluid dynamic," *JTTM J. Terap. Tek. Mesin*, vol. 4, no. 2, pp. 207–214, 2023, doi: 10.37373/jttm.v4i2.633.

[50] T. J. Erinle, S. O. Ejiko, and D. H. Oladebeye, "Design of Micro Hydro Turbine for Domestic Energy Generation," *Iarjset*, vol. 7, no. 4, pp. 85–93, 2020, doi: 10.17148/iarjset.2020.7414.

[51] N. Acharya, C. G. Kim, B. Thapa, and Y. H. Lee, "Numerical analysis and performance enhancement of a cross-flow hydro turbine," *Renew. Energy*, vol. 80, pp. 819–826, 2015, doi: 10.1016/j.renene.2015.01.064.

[52] V. Sammartano, G. Morreale, M. Sinagra, and T. Tucciarelli, "Numerical and experimental investigation of a cross-flow water turbine," *J. Hydraul. Res.*, vol. 54, no. 3, pp. 321–331, 2016, doi: 10.1080/00221686.2016.1147500.

[53] S. C M and V. Madav, "Numerical and experimental investigation of modified V-shaped turbine blades for hydrokinetic energy generation," *Renew. Energy*, vol. 177, pp. 1170–1197, 2021, doi: 10.1016/j.renene.2021.05.086.

[54] C. M. Shashikumar, V. Hindasageri, and V. Madav, "CFD investigation of unsteady three-dimensional savonius hydrokinetic turbine in irrigation channel with varying positions for hydro power application," *AIP Conf. Proc.*, vol. 2316, 2021, doi: 10.1063/5.0036472.

[55] W. C. Schleicher, J. D. Riglin, and A. Oztekin, "Numerical characterization of a preliminary portable micro-hydrokinetic turbine rotor design," *Renew. Energy*, vol. 76, pp. 234–241, 2015, doi: 10.1016/j.renene.2014.11.032.

[56] I. F. S. dos Santos, R. G. R. Camacho, and G. L. Tiago Filho, "Study of the wake characteristics and turbines configuration of a hydrokinetic farm in an Amazonian river using experimental data and CFD tools," *J. Clean. Prod.*, vol. 299, p. 126881, 2021, doi: 10.1016/j.jclepro.2021.126881.

[57] S. C M, R. Honnasiddaiah, V. Hindasageri, and V. Madav, "Experimental and numerical investigation of novel V-shaped rotor for hydropower utilization," *Ocean Eng.*, vol. 224, no. April 2020, p. 108689, 2021, doi: 10.1016/j.oceaneng.2021.108689.

[58] A. Hamad, S. M. A. Aftab, and K. A. Ahmad, "Reducing Flow Separation in T-Junction Pipe Using Vortex.pdf," *J. Adv. Res. Fluid Mech. Therm. Sci.*, vol. 1, no. 1, pp. 36–46, 2018.

[59] S. Shoeibi, N. Rahbar, A. A. Esfahlani, and H. Kargarsharifabad, "Energy matrices, exergoeconomic and enviroeconomic analysis of air-cooled and water-cooled solar still: Experimental investigation and numerical simulation," *Renew. Energy*, vol. 171, pp. 227–244, 2021, doi: 10.1016/j.renene.2021.02.081.

[60] C. Gnanavel, R. Saravanan, and M. Chandrasekaran, "CFD analysis of solar still with PCM," *Mater. Today Proc.*, vol. 37, no. Part 2, pp. 694–700, 2020, doi: 10.1016/j.matpr.2020.05.638.

[61] A. H. Alami and H. Bilal, "Experimental Evaluation of a Buoyancy Driven Energy Storage Device," *Adv. Mater. Res.*, vol. 816–817, pp. 887–891, 2013, doi: 10.4028/www.scientific.net/AMR.816-817.887.

[62] J. N. Fernando and D. E. Rival, "Characterizing the influence of upstream obstacles on very low head water-turbine performance," *J. Hydraul. Res.*, vol. 52, no. 5, pp. 644–652, 2014, doi: 10.1080/00221686.2014.917809.

Dan Mugisidi - Effect of buoyancy force on buoyancy waterwheel efficiency using numerical flow simulation

ORIGINALITY REPORT

11%	7%	7%	2%
SIMILARITY INDEX	INTERNET SOURCES	PUBLICATIONS	STUDENT PAPERS

PRIMARY SOURCES

1	www.mdpi.com Internet Source	2%
2	lbk.be Internet Source	1%
3	Wenjin Feng, Yuan Zheng, An Yu, Qinghong Tang. "Experimental and Numerical Analysis of the Clearance Effects between Blades and Hub in a Water Wheel Used for Power Generation", Water, 2022 Publication	1%
4	Submitted to Modern College of Business and Science Student Paper	<1%
5	Oktarina Heriyani, Dan Mugisidi, Irfan Hilmi. "Effect of the surface of the rough pipe on the fluid flow rate", IOP Conference Series: Materials Science and Engineering, 2020 Publication	<1%
6	Emanuele Quaranta, Jean Pierre Perrier, Roberto Revelli. "Optimal design process of	<1%

	crossflow Banki turbines: Literature review and novel expeditious equations", Ocean Engineering, 2022 Publication	
7	www.researchgate.net Internet Source	<1 %
8	Submitted to University of Queensland Student Paper	<1 %
9	link.springer.com Internet Source	<1 %
10	semarakilmu.com.my Internet Source	<1 %
11	Submitted to Case Western Reserve University Student Paper	<1 %
12	Emanuele Quaranta, Roberto Revelli. "Output power and power losses estimation for an overshot water wheel", Renewable Energy, 2015 Publication	<1 %
13	www.iksadkongre.net Internet Source	<1 %
14	arxiv.org Internet Source	<1 %
15	Vimal N. Chaudhari, Samip P. Shah. "Performance enhancement of savonius	<1 %

hydrokinetic turbine using split airfoil blade: A numerical investigation", Renewable Energy, 2024
Publication

16	dergipark.org.tr Internet Source	<1 %
17	journal.hydrogen.or.kr Internet Source	<1 %
18	Ashok Kumar Sahoo, Virendra Patel. "Augmenting mechanical properties of friction stir welded AA1100 by reinforcing SiC/Al2O3particulates", Materials Today: Proceedings, 2020 Publication	<1 %
19	Chunxia Yang, Qian Li, Xueyuan Hu, Yuan Zheng, Jiawei Wu, Shengzhi Su, An Yu. "Fish injury analysis and flip-blade type optimization design of an undershot waterwheel", Renewable Energy, 2023 Publication	<1 %
20	Nusrat Jahan Bipa, Giulia Stradiotti, Maurizio Righetti, Giuseppe Roberto Pisaturo. "Impacts of hydropeaking: A systematic review", Science of The Total Environment, 2024 Publication	<1 %
21	Qidun Maulana Binu Soesanto, Anjar Susatyo, Puji Widiyanto. "Performance optimization of	<1 %

axial-flow hydraulic turbine using artificial bee colony (ABC) algorithm", 2017 International Conference on Sustainable Energy Engineering and Application (ICSEEA), 2017
Publication

---

22 Susastro Susastro, Ardi Noerpamoengkas, Miftahul Ulum, Gatot Setyono. "Performance Analysis of Wind Power Generation Models Using Oscillating Water Column", JRST (Jurnal Riset Sains dan Teknologi), 2020 — <1%
Publication

---

23 Tomomi Uchiyama, Shou Uehara, Haruki Fukuhara, Shouichiro Iio, Toshihiko Ikeda. "Numerical study on the flow and performance of an open cross-flow mini-hydraulic turbine", Proceedings of the Institution of Mechanical Engineers, Part A: Journal of Power and Energy, 2015 — <1%
Publication

---

24 kipdf.com — <1%
Internet Source

---

25 ruor.uottawa.ca — <1%
Internet Source

---

26 spectrum.library.concordia.ca — <1%
Internet Source

---

27 Mengshang Zhao, Yuan Zheng, Chunxia Yang, Yuquan Zhang, Qinghong Tang. "Performance — <1%

Investigation of the Immersed Depth Effects on a Water Wheel Using Experimental and Numerical Analyses", Water, 2020
Publication

28 D Mugisidi, O Heriyani, H Fathurahman. "Comparison of plastic and stainless-steel as solar still material", IOP Conference Series: Materials Science and Engineering, 2018 <1%
Publication

29 F. R. Menter. "Two-equation eddy-viscosity turbulence models for engineering applications", AIAA Journal, 1994 <1%
Publication

30 Yaowared Khonkhem, Suabsagun Yooyuanyong. "Finite difference for magnetic field response from a two-dimensional conductive ground", Applied Mathematical Sciences, 2016 <1%
Publication

Exclude quotes	Off	Exclude matches	Off
Exclude bibliography	On		